Groundwater for the North of Namibia

Volume I b

Kalahari Research Project

Results of Analysis
from Drill Holes on the
Cubango Megafan

BGR Bundesanstalt für Geowissenschaften und Rohstoffe

Editor: Falk Lindenmaier
Authors and contributing Persons: (in alphabetical order):
Harald G. Dill, Reiner Dohrmann, Juliane Fenner, Ulrich Gersdorf, Stephan Kaufhold, Robert Kringel, Falk Lindenmaier, Rolf-Rüdiger Ludwig, Roy McG. Miller, Andrea Nick, Ursula Noell, André Walzer.

Research Project of the Federal Institute for Geosciences and Natural Resources:
„Entwicklung und Alterseinstufung von Duricrusts als Basis für die paläogeografische und -hydrogeologische Modellierung im Cuvelai-Etosha-Becken in Nord-Namibia“.

Translated Title: “Development and Dating of Duricrusts as base for a paleogeographic and hydrogeological model of the Cuvelai-Etosha Basin in North Namibia”.

BGR-Archive No.:

Date: February 2012

Report Series of Volume I

Executive Summary: Groundwater for the North of Namibia – Phase I

Part A: Groundwater for the North of Namibia: Summary Report of Activities of Phase I - Exploration of Ohangwena II Aquifer and Preliminary Isotope Study

Part B: Kalahari Research Project: Results of Analysis from Drill Holes on the Cubango Megafan

Part C: Groundwater for the North of Namibia: Summary Report on the Hydrocensus carried out in the Northern Namibian Part of the Cuvelai-Etosha Basin

Part D: Groundwater for the North of Namibia: Groundwater Exploration with TEM-soundings in the Cuvelai-Etosha Basin

Content

Appendix

Abbreviations

General Abbreviations

BGR	Federal Institute of Geosciences and Natural Resources of Germany
BMZ	German Federal Ministry for Economic Cooperation and Development
CEB	Cuvelai-Etosha Basin
DWA-BGR	Groundwater Investigation of the Cuvelai-Etosha Basin of Federal Institute of Geosciences and Natural Resources of Germany (BGR) and the Department of Water Affairs and Forestry (DWAF)
DWAF	Department of Water Affairs and Forestry
GROWAS	Database to store groundwater relevant points at DWAF
MAWF	Ministry of Agriculture, Water and Forestry
KDP / KOH-0	Discontinuous Perched Aquifer
KOH-1	Upper Ohangwena Aquifer
KOH-2	Lower Ohangwena Aquifer

Technical Abbreviations

a	year
m bgl	Meter below surface
m asl	Meter above sea level
TEM	Transient electromagnetic method
SRTM	Shuttle Radar Topography Mission
ASTER	Advanced Spaceborne Thermal Emission
XRD	X-Ray Diffractometry
DTA-MS	Thermoanalytical investigation
XRF	X-Ray Fluorescence Analysis
CEC	Cation Exchange Capacity
IR	Infrared Spectroscopy
ESEM	Scanning Electron Microscope
ICP-MS	Inductively coupled plasma mass spectrometry
ICP-OES	Inductively coupled plasma optical emission spectrometry
AAS	Atomic absorption spectroscopy
IC	Ion chromatography
TDS	Total dissolved solids (mg/L)
TOC	Total organic carbon (mg/L)
DOC	Dissolved organic carbon
DO	Dissolved oxygen (mg/L)
EC	Electric Conductivity (µS/cm; mS/cm)
EN	Electroneutrality (%)

Abstract

Within the technical cooperation project “Groundwater for the North of Namibia”, funded by the European Union and the Bundesministerium für Wirtschaftliche Zusammenarbeit und Entwicklung (BMZ), exploratory drilling was conducted to a depth of 400 m in parts of the Cubango Megafan. In order to get a better picture of the sedimentological and hydrogeological genesis of the Owambo Basin and especially in the Cubango Megafan, a research project, funded by the Bundesanstalt für Geowissenschaften und Rohstoffe (BGR) was initiated to investigate samples and core sections that were retrieved in above mentioned drillings. For this project, a first set of samples from flushing of mud rotary drills and core drill sections were analyzed by different methods and resulted in several short reports and data collections. These were combined in this report to have both a general and detailed overview.

The accessory appendix contains many tables and figures of these and additional investigations. An additional product of these analyses is the publication of Dill et al. (2012). A second set of samples is currently investigated. Due to the fact that sample investigation is ongoing and further publications are already in preparation the discussion and conclusions are kept rather short.

1 Introduction

The Cuvelai-Etosha Basin (CEB) is a huge sedimentary system located in southern Angola and northern Namibia, it spans about 165.000 square kilometers. The Etosha Pan, as the primary depression and collector for surface water is the topographic center of the CEB. In the north it is flanked by two river systems, the Kunene and the Cubango River, which in former times contributed to the Paleolake Etosha. These two river systems and the Paleolake Etosha dominated the complex sedimentary system of the CEB since approximately the early Tertiary. North-East of the Etosha Pan, the so called Cubango Megafan is focus of this research project.

This document contains results of supplemental research that accompanies the below mentioned technical cooperation project and is funded by a research project of the Federal Institute for Geosciences and Natural Resources (BGR), Germany. The project is called the “Kalahari Project” within this document. Many samples were taken to the laboratories of BGR and were investigated for different characteristics. Some short reports were written but other results only documented in Excel sheets. This report combines all results until December 2011 and gives an overview of activities. Besides this report a publication in the International Journal of Earth Sciences is placed, including additional investigative work (Dill et al., 2012).

Since 2007, the German-Namibian Technical Cooperation project "Groundwater for the North of Namibia" is aimed to support groundwater management purposes for groundwater systems of the Cuvelai-Etosha Basin. The technical cooperation project is carried out by the Department of Water Affairs and Forestry (DWAF) and BGR. It is referred to as the DWA-BGR Project in this text.

The technical cooperation project kindly provided samples from rotary drilling and core drilling campaigns for further investigation at BGR. As a matter of fact this means that results presented here are closely linked to activities that are described in the summary report of the technical cooperation project of phase I (Part A of this series of reports). The aim is to shed light on the sedimentary history of the CEB with a focus on the Cubango Megafan, a special sedimentary structure in the east of the CEB. With the results and understanding of the sedimentary system it is aimed to improve the understanding of the hydrogeological system of the Cubango Megafan. This finally will help to distinguish between salt and freshwater resources and to support quantification and qualification of the resources for groundwater management purposes.

The appendix combines results of both report parts A and B.

Most of the pumping wells that were drilled on the Cubango Megafan have a maximum depth of 150 to 200 meters and were the only available source for subsurface interpretation. A few deeper boreholes do exist, however data and reports of these usually lack important information for a detailed hydrogeological interpretation.

The need for a more detailed investigation of the sediment column was identified readily by Bittner and Klezcar (2006) and Zauter (personal communication) and led to a more focused investigation including some well recorded mud rotary drills as well as core drills within the realm of the Cubango Megafan. Samples of the drillings were shipped to BGR laboratories for mineralogical, paleontological and sedimentological investigation. From February to March 2009, a first drilling campaign with a rotary mud drilling method resulted in three deep seated boreholes in the Cubango Megafan. The three boreholes WW201045-WW201047 reached depths of up to 400 m and stroke fresh groundwater in depths of 200-300 m.

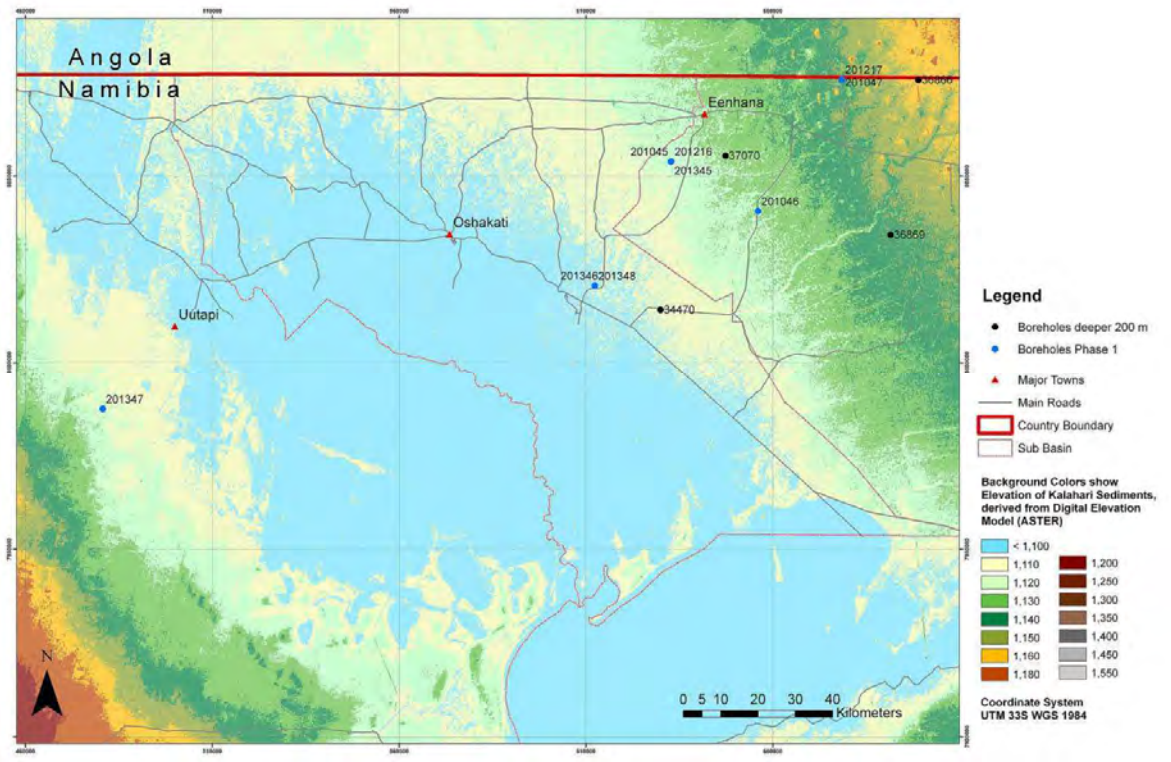

Figure 1: Location of boreholes of drilling campaign I to III

- Borehole WW201046: only 6 samples of cuttings were shipped to BGR, grain size distribution was analyzed for these samples.
- Borehole WW201045: 66 samples of cuttings were shipped to BGR. Following analyses were done for these samples: grain size distribution, main and trace elements (X-ray fluorescence analysis). Additional sample investigation was

conducted for a publication (Dill et al., 2012) and is listed within this publication. During recovery of the drill head, clayey sediment was retrieved which stuck at the drill head and was fully analyzed separately to other samples. It is assumed that this clayey sediment belongs either to the Ombalantu Formation or the Karoo Group that was hit by the drill head but not recovered in the cuttings.

From May to July 2009, a drilling campaign was conducted that resulted in two cored boreholes each near to existing borehole locations of WW201045 and WW201047. From these two boreholes 10 core sections were selected from each and send to BGR in July 2009. These were analyzed for grain size distribution, mineralogical and chemical content, but also for pore fluid content and bulk resistivity. Determination of hydraulic parameters (Walzer, 2010) was conducted as well, but is described in chapter 6.3 of report Part A. It was originally planned to use calcrete from the core drill samples for age determination with isotopes. This proved to be not feasible, as material that could tidily be separated from the main samples was too little for investigation. In Table 1, an overview of all activities and sub-reports with date of finish concerning the Ohangwena II aquifer is given. Some of the reports are also integrated into this summary report.

In 2011, further core sections were sent to BGR, these are still under investigation.

Table 1: Overview of activities, results and reports that were conducted in Phase I.

Type	Description	Time conducted	Location of data or report	Data Format
Desk Study Report: Cuvelai-Etosha Groundwater Investigation	Extended report of general geographical and geological situation of the CEB	2006	Appendix 1	Pdf
TEM soundings	Pictures of TEM soundings and Report Part C	10-2008	Part C Appendix 2	Pdf WMF
Drilling campaign I: 201045, 201046, 201047				
General Information	Drilling report for three deep boreholes in Cuvelai-Etosha Basin, including lithology, hydraulic tests, chemistry, well structure Detailed lithology description (Miller)	03-2009	Part A Appendix 1 Appendix 3	Pdf Excel Excel
Hydrochemistry	Windhoek Lab Excel Sheets	05-2009	Appendix 1 Appendix 8	Excel
Mineralogy and Sedimentology	Analysis of lowest clay sample of 201045 Grain size distribution, XRF, XRD and Heavy Minerals of crushed samples	07-2009 06-2009 12-2010	Part B Appendix 4	Pdf Excel
Micropaleontology	Short report for diatoms of lowest clay sample (Fenner)	06-2009	Part B	Pdf
Drilling campaign II: Core drills 201216 and 201217				
General Information	Drilling report: included in thesis of Walzer) Detailed lithology description (Miller) Litholog and core-photos (Gersdorf)	03-2010 04-2010	Part B Appendix 1 Appendix 4	Pdf Excel Pdf
Mineralogy etc.	Full analysis of core samples 201216, 201217 (Walzer, Kaufhold et al.: BGR Lab)	01-2010 05-2010	Part B	Pdf
Micropaleontology	report: Silt fraction analysis for minerals, fossils (Fenner)	04-2010	Part B	Pdf
Hydraulics	Core sample hydraulic investigation (included in thesis of Walzer)	03-2010	Part A Appendix 1	Pdf
Drilling campaign III: 201345-201348				
General Information	Drilling report including lithology, hydraulic tests, chemistry, well structure (van Wyk)	03-2010	Part A Appendix 1	Pdf Excel
Hydrochemistry	Windhoek Lab Excel Sheets (Rügheimer)	04-2010	Part A Appendix 1 Appendix 8	Excel
Geophysical Campaigns				
Campaign I: Terratec	Geophysical Logging in the CEB (report: Terratec, Symons)	09-2009	Part A Appendix 6	Pdf WCL
Campaign II: Poseidon	Logging was conducted but no report delivered, raw data available	03-2010	Part A Appendix 7	WCL
Additional activities				
3D Model Ohangwena II	3D Model Ohangwena II based on TEM soundings (Zeilfelder)	06-2009	Part A	Pdf
Isotope Study	Tritium, H-2, O-18, C-14 (Nick, Lindenmaier)	12-2009	Part A	Pdf
Groundwater recharge	Master Thesis on Groundwater recharge (Starke, in German)	04-2010	Appendix 1	Pdf

2 Summary of the geology of the Cuvelai-Etosha Basin

By André Walzer and Falk Lindenmaier

The geology of the Namibian part of Cuvelai-Etosha basin has been most extensively described by Miller (2008b) and Miller (2010), and most of the information comprised here is from these sources. An overview of the geology of the CEB catchment area that comprises the CEB and parts of Kunene and Cubango Rivers is shown in Figure 2. With regard to development and efforts made in the first Phase of the DWA-BGR Project on the Ohangwena II Aquifer, the report will focus on the north-eastern region of the CEB, and hence lies within the Ohangwena Region.

As the onset of the Kalahari sedimentation is uncertain, it was set at the end of the Cretaceous or the beginning of the Tertiary. It is marked that degradation and active incision gradually gave way to aggradation and deposition as the older Karoo rocks were exposed and subject to erosion and weathering before sedimentation resumed. Hence, the base of Kalahari probably is heavily incised with bedrock of Karoo or older formations which may consist of more than 50 m of weathered surface rock in some areas (Miller, 2008b, p 24-5). The depositional environment of the CEB was dominated by calcrete development in the southern and western margins. In the north, the Kunene and Cubango-Okavango river systems dominated a clastic sedimentary environment.

For the past 70 Ma years, the Owambo Basin has been filling up with sand, silt and clay that was eroded from higher grounds surrounding the area. For sediments within the Ohangwena Region, mountains in central Angola contributed to the sedimentary material (Figure 2) but also a considerable amount of Kalahari sediments might have been reworked. Cycles of climate change with wet and dry periods followed each other (Mendelsohn et al., 2000). The Etosha Lake must have had different extensions and water depths or might have been dry. Rivers drained into the basin bringing sedimentary deposits with them, called the Ombalantu, Beiseb, Olukonda and Andoni formations (Miller, 2008b). Aeolian components are also found. Ombalantu represents the base and Andoni the top of the named formations. These four formations form the youngest unit of the basin and are part of the Kalahari Sequence. The following lithological and stratigraphical descriptions of the Kalahari formations are based on the work of Miller (Miller, 2008b; Miller, 1997; Miller et al., 2010) and mainly consider the sediments and distribution within the Cuvelai-Etosha Basin as part of the larger Owambo Basin.

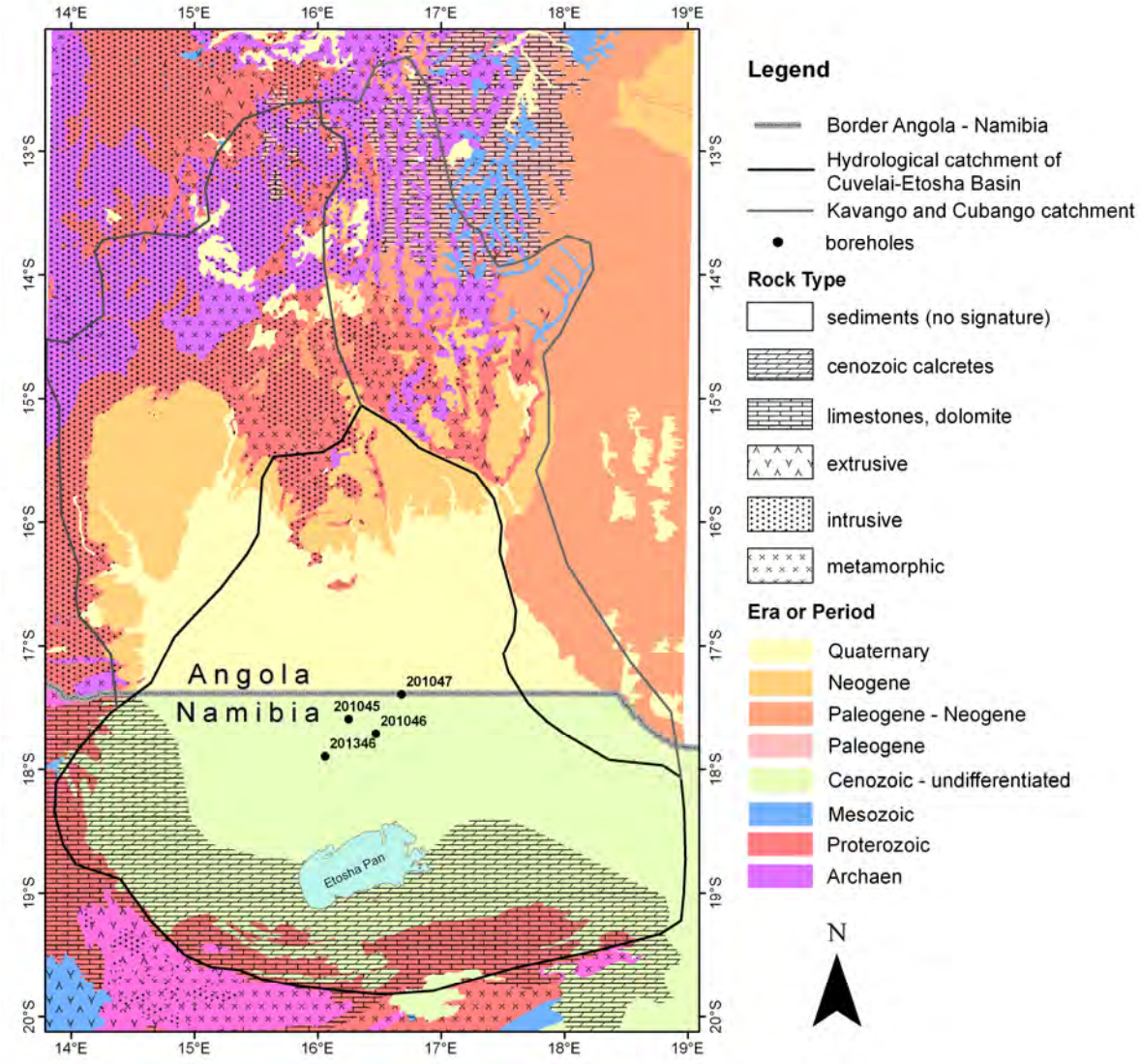

Figure 2: Overview of the geology of the CEB – from the Digitized Carta Geológica de Angola 1:1.000.000 (de Araújo et al., 1988) and the Simplified Geological Map of Namibia (1:2.000.000) (Geological Survey of Namibia). The major drilling sites of the DWA-BGR project are also shown, not all drilled boreholes are mentioned as some were drilled near to each other.

Miller (2008b) states that during the whole time since the Cretaceous the still-existing depression of the basin existed and contained lakes according to the climatic circumstances. Generally, the Kalahari Succession might thicken to about 600 m to the north, respective towards the Angolan border but thins eastwards to the pre-Kalahari basement outcrops along the Okavango River (Figure 3a) according to Miller (2008b). A discrepancy to his figure is found in figures of Haddon (2005) (Figure 3b) and the geological maps of Angola and Namibia (de Araújo et al., 1988; Miller and Schalk, 1980) who describe smaller depths of up to 450 m with a depression center where the DWA-BGR project boreholes were drilled (Figure 4).

Much of the sediment in the Owambo Basin is largely unconsolidated or only partially consolidated and appears to have been deposited by the sand-dominated Cubango Megafan in the east and the much smaller, mud-dominated Kunene megafan in the west. Some cemented sands are logged as sandstones in some archive borehole logs, although cementing is usually limited and weak. Exactly when Kalahari deposition began and what constitutes the base of the Kalahari in the Kalahari basin is not well defined, the lowest Ombalantu formation could be Cretaceous or early Tertiary. In Namibia, Botswana and South Africa, the base of the Kalahari Group is taken as the first unconsolidated or semi-consolidated sediments that overlie solid basement rocks, commonly of the Karoo Supergroup.

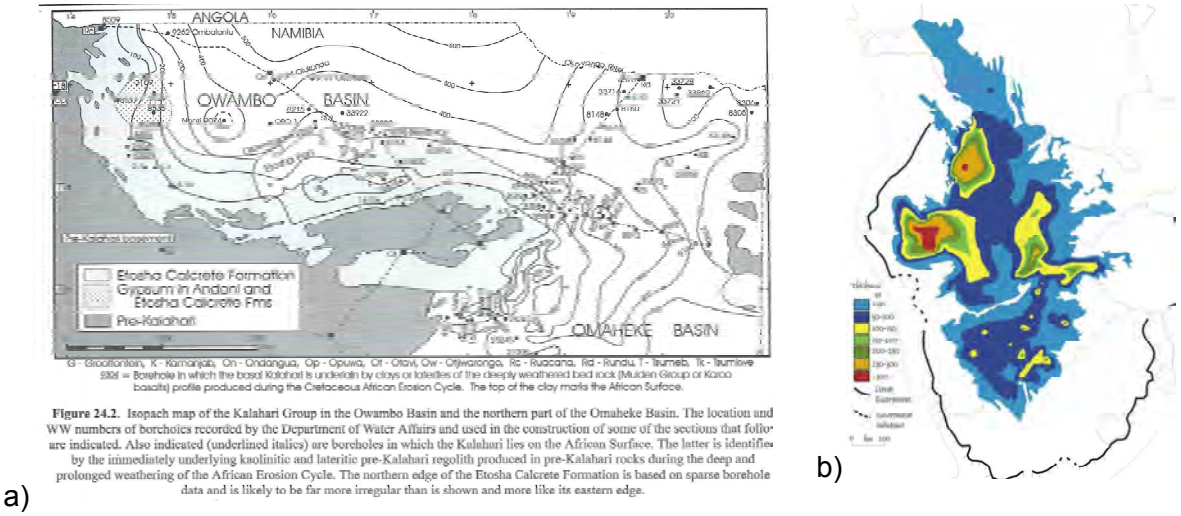

Figure 24.2. Isopach map of the Kalahari Group in the Owambo Basin and the northern part of the Omaheke Basin. The location and WW numbers of boreholes recorded by the Department of Water Affairs and used in the construction of some of the sections that follow are indicated. Also indicated (underlined italics) are boreholes in which the Kalahari lies on the African Surface. The latter is identified by the immediately underlying kaolinitic and lateritic pre-Kalahari regolith produced in pre-Kalahari rocks during the deep and prolonged weathering of the African Erosion Cycle. The northern edge of the Etosha Calcrete Formation is based on sparse borehole data and is likely to be far more irregular than is shown and more like its eastern edge.

Figure 3: a) Isopach map from (Miller, 2008b) of Kalahari sediment depth and b) estimated Kalahari sedimentary depths in the Great Escarpment of Southern Africa. The figure was taken from (Hipondoka, 2005) but is a map of (Haddon, 2005), showing that the Owambo Basin has the thickest Kalahari sedimentary deposits and that the Ohangwena Region is located at the eastern border of this largest depression (red).

Ombalantu Formation - A basal, red, fine-grained, semi-consolidated but friable formation with variably silicified mudstones but almost entirely consisting of clay. Formerly it has been described as “sandstone” or “siltstone” but in fact it is a mudstone with varying grades of silicification. Some silt and sand is found and at the base it might contain pebbles (borehole WW9296). It does not crop out and it has a broad elongate distribution extending from the south-east to the north-west of the basin and reaches a maximum thickness of 80 m. According to Miller (2008b: figure 24.8) it does not necessarily exist in the Ohangwena Region but this might also be due to inadequate depths of existing boreholes. Gypsum and Gypsum crystals occur in the upper part of the formation. Miller (Miller, 2008b) evaluates its deposition to be mainly from the accumulation of fine clastics

in a shallow, low energy, deltaic environment. A restricted continental basin with a significant and sufficient amount of evaporation was required to lead to the appearance of gypsum.

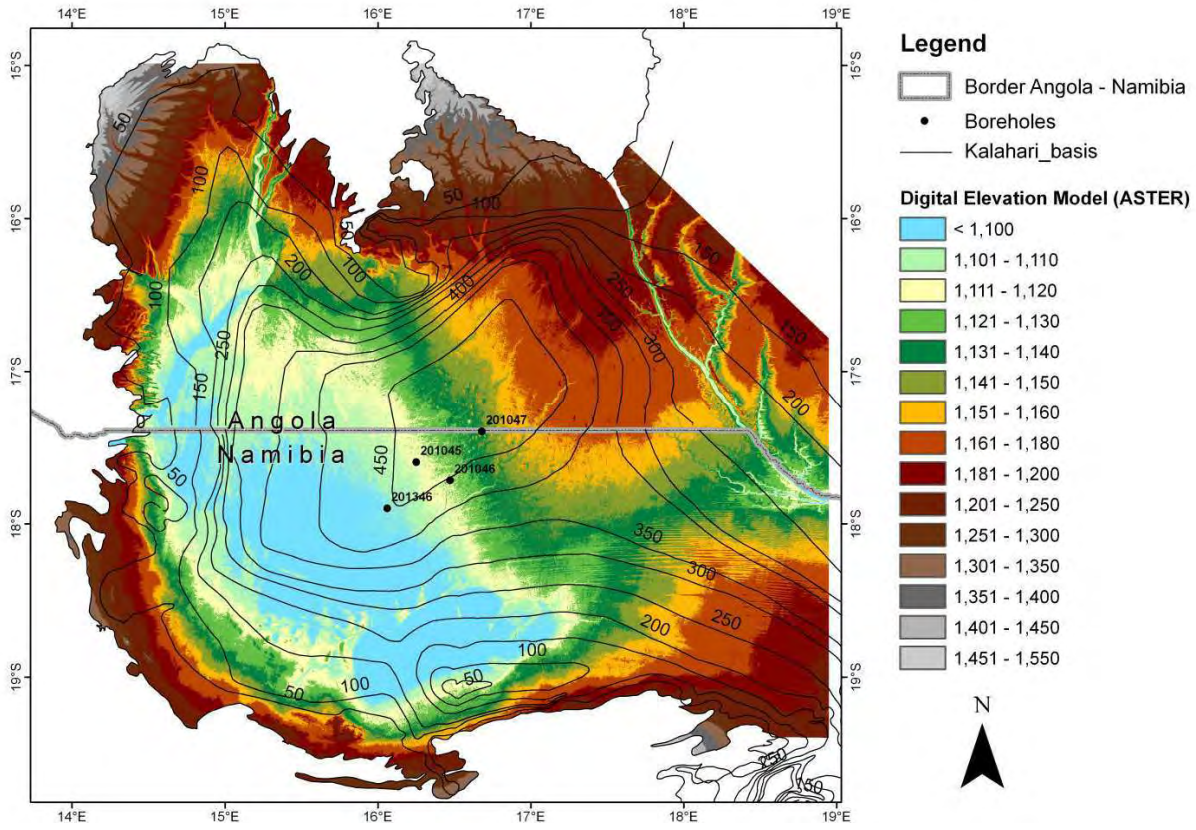

Figure 4: Digital elevation of the Kalahari Sediments in the CEB and parts of Kunene and Cubango Catchments. The basis the Kalahari Formation is displayed with depth contour lines from the geological maps of Namibia and Angola (de Araújo et al., 1988; Miller and Schalk, 1980), please note the varying scale of surface elevation.

The Beiseb Formation is a gravel deposit which is widespread, generally reddish in color and represents a period of rapid and extensive input of material from the basin margins. It consists of well rounded sand and clay stone clasts which are set in a matrix of fine to medium grained, argillaceous, and calcareous to dolomitic sandstone. With a maximum thickness of 47 m, it is the thinnest of the Kalahari Formations (Miller, 2008b).

Olukonda Formation - A friable, poorly consolidated, reddish brown, poorly sorted massive sand and sandstone formation with a limited distribution but a broad elongate sub-outcrop similar to the Ombalantu Formation. It contains a few thin gritty and pebbly layers and is up to 152 m thick. Bittner (2006) describe the principal layering in the Cubango Megafan area and allocates the freshwater containing sands below the aquitard to the Olukonda formation.

Andoni Formation - It occurs throughout the Owambo Basin as a cover to all underlying units and consists of inter-bedded white medium grained sand, light greenish clayey sand and green clay. In zones, the predominant sand varies in thickness between 10 and 200 m and shows an unconsolidated, slightly pyritic or hematitic condition. The top part of the section contains numerous irregular-shaped dolocrete and calcrete nodules which are embedded in polished, angular to sub-rounded grains of quartz which in turn make up to 90 % of the sand. Sorting improves upwards in the sequence. The appearance of clay layers within this formation varies in thickness between a few centimeters and 150 m (Ombalantu borehole in Miller (Miller, 2008a)). They are often silty and/or sandy. Around the Etosha pan, different lithologies are found in the Andoni Formation, for further details see Miller (Miller, 2008a).

A significant contribution to the sedimentary evolution of the CEB is written by Miller (2008a; page 24-12) and is cited here in full to contribute to the discussion of findings in this report: “The occurrence of a clay-rich zone separating an upper brackish aquifer from a lower freshwater aquifer (author: possibly within the Andoni formation) may well be a rather general feature of the regional Cubango-Okavango and the Kwando Rivers and their fan systems since that same superposition of aquifers with an intervening aquitard occurs east of the Kwando river in the Caprivi. The intersected parts of the sand-rich Cubango Megafan contrast markedly with the clay-rich Andoni and Olukonda Formations in the western parts of the Owambo Basin (…). This contrast seems to illustrate a marked difference between the Paleo - Kunene depositional system and the Cubango Megafan, the former mud dominated and the latter sand dominated. Another surprising and significant difference is the fact that although the catchment of the Kunene system in Angola is not significantly smaller than that of the Cubango system, the Kunene fan is nowhere near as large and well developed as the Cubango Megafan, even where the Kunene system emerges from the confining highlands in the region of 17°S (…). In fact, there is no obvious Kunene megafan and although the Kunene is considered in this volume to have contributed a significant amount of sediments to the Owambo Basin, an alternative consideration is that the clays in the western part of the Owambo Basin are, instead, the distal deposits of the Cubango Megafan”, end citation.

3 Mineralogy and geochemistry of selected samples

By Reiner Dohrmann, Stephan Kaufhold, Robert Kringel, Falk Lindenmaier and Ursula Noell

The boreholes of campaign 1 to 3 are so far the best recorded boreholes in the Ohangwena Region and on the Cubango Megafan and its vicinity; especially the cored boreholes are a novelty there. So a more extensive investigation of soil samples seemed to be obvious, especially to get knowledge about sedimentation history and genesis of aquitards and aquifers. The following chapter describes data from lab results and summarizes several reports (Kaufhold and Dohrmann, 2009a; Kaufhold and Dohrmann, 2009b; Kaufhold and Dohrmann, 2010).

Samples of cuttings were retrieved of rotary boreholes WW201045 and WW201047. These samples were analyzed for their grain size distribution and a selection of samples were analyzed with X-ray fluorimetry (XRF) and enriched for light heavy mineral analysis. A clay sample analysis from the drill head was also analyzed after it was finally retrieved after drilling stopped in WW201045.

From the cored boreholes a pre-selection of cores was taken in Windhoek and these parts were sent to BGR laboratories. A wide spectrum of analyzes was conducted there on 9 samples of WW201216 and 11 samples of WW201217. Besides mineralogical and geochemical investigation, micropaleontology, hydraulic conductivity, pore-water content and bulk material conductivity was measured. The results of these investigations are found in more detail in several short reports (Appendix 1) and are comprised in the following chapters.

3.1 Methods

his chapter is an extract of following reports (Kaufhold and Dohrmann, 2009a; Kaufhold and Dohrmann, 2009b; Kaufhold and Dohrmann, 2010). For sample preparation, in general, 10 g from the drill cores were dried at 60°C and ground by a mortar mill. Following methodologies were applied to the samples

3.1.1 X-Ray Diffractometry, XRD

XRD pattern were recorded using a Philips X´Pert PW3710 Θ-2Θ diffractometer (Cu-Kα radiation generated at 40 kV and 40 mA), equipped with a 1° divergence slit, a secondary monochromator, a point detector and a sample changer (sample diameter 28 mm). The samples were investigated from 2° to 80° 2Θ with a step size of 0.02° 2Θ and a

measuring time of 3 sec per step. For specimen preparation the top loading technique was used.

3.1.2 Thermoanalytical investigation, DTA-MS

Thermoanalytical investigations were performed using a Netzsch 409 PC thermobalance equipped with a DSC/TG sample holder linked to a Pfeiffer Thermostar quadrupole mass spectrometer (MS). 100 mg of powdered material previously equilibrated at 53 % relative humidity (RH) was heated from 25 -1000°C with a heating rate of 10K/min.

3.1.3 X-Ray Fluorescence Analysis, XRF

The chemical composition of powdered samples was determined using a PANalytical Axios and a PW2400 spectrometer. Samples were prepared by mixing with a flux material and melting into glass beads. The beads were analyzed by wavelength dispersive X-ray fluorescence spectrometry (WD-XRF). To determine loss on ignition (LOI) 1000 mg of sample material was heated to 1030 °C for 10 min.

3.1.4 Organic Carbon, LECO

The organic carbon (OC) content was measured with a LECO CS-444-Analysator after dissolution of the carbonates. Carbonates had been removed by treating the samples several times at 80 °C with HCl until no further gas evolution could be observed. Samples of 170-180 mg of the dried material were used to measure the total carbon (TC) content. TIC was calculated by the difference of TC-TOC. The samples were heated in the device to 1800-2000 °C in an oxygen atmosphere and the CO2 was detected by an infrared detector.

3.1.5 Cation Exchange Capacity, CEC

The CEC was measured using the Cu-Triethylenetetramine method (Meier and Kahr, 1999).

3.1.6 Infrared Spectroscopy, IR

For measuring mid (MIR) infrared spectra the KBr pellet technique (1 mg sample / 200 mg KBr) was applied. Spectra were collected on a Thermo Nicolet Nexus FTIR spectrometer (MIR beam splitter: KBr, detector DTGS TEC; FIR beam splitter: solid substrate, detector DTGS PE).

3.1.7 Scanning Electron Microscope Pictures ESEM

For SEM investigation a FEI Quanta 600 F operated in low-vacuum mode (0.6 mbar) was used. Therefore, sputtering of the samples with gold or carbon is not necessary. The microscope is equipped with the EDX-system Genesis 4000 of EDAX.

3.1.8 Porosity (bulk and specific density)

The bulk or envelope density was determined from the air dried samples with a micromeritics GeoPyc 1360. This pycnometer utilizes a free-flowing, finely divided, dry powder as the fluid medium instead of a liquid. The hard, spherical and small particles do not enter pores < 50 µm but do envelop the irregular shape of the crushed clay particles. Samples of about 10 to 15 g were used (Webb and Orr, 1997). The specific density (or absolute density) was determined from samples dried at 105 °C for 2 d until no further weight change was observed. The sample weights were about 12 g. The pycnometer was a helium pycnometer AccuPyc 1330 of micromeritics. The sample volume is calculated from the observed pressure change the helium undergoes when it expands from one chamber containing the sample into another chamber without sample (Webb and Orr, 1997). The difference of bulk and specific density is caused by the porosity which in turn can be calculated considering both types of density (Webb and Orr, 1997).

3.1.9 Grain Size Analysis with a Sedigraph

Grain size analysis was performed using X-ray granulometry (XRG): SediGraph 5100™ with MasterTech 052 Autosampler™ (Micrometrics, Norcross, Georgia, USA). The device is used to measure gravity-induced settling rates of different size particles through X-ray absorption of particles in a suspension. Prior to this measurement, the samples were dispersed in a 0.01 N Na2P2O7 * 10 H2O solution, and fraction > 63 µm was subjected to drying and conventional sieving. All material which passed the 63 µm sieve was freeze-dried and re-suspended to fit the requirements of XRG regarding solution/solid ratio. This procedure also included ultrasonic treatment of the suspension (2 x 2 min at 20 kHz) plus a weak ultrasonic short-shake-up just prior to XRG measurement.

3.1.10 Elution production and pore fluid element analysis

An elution of a soil sample is made to extract the soluble pore element content. It is a representation of the content of the pore fluids. Twenty-five milliliters of de-ionized water is added to 10 g of a sample. After one hour, the electrical conductivity (Eh) and the pH-Value are determined. The weight proportion of solid matter to the liquid is 1:2.5. In a second step, additional 25 ml of de-ionized water is added and measurement of Eh and pH is repeated which results in a weight proportion of 1:5. In a third step, additional 50 ml

of de-ionized water is added, a weight proportion of 1:10 is reached. This is equivalent to a standardized procedure for elution in Germany (DIN EN 12457-4, 2003). The elution 1:10 was centrifugalized (30 min/4000 UpM) and filtrated (0.45 µm). The anions were determined with an IC (ion-chromatograph) and the cations were determined with an ICP-OES. The resulting concentrations in the elution 1:10 are referred to the solid matter in mg/kg (Kringel and Hoffmann, 2008).

3.1.11 Spectral induced polarization method (SIP) to determine bulk rock electrical conductivity

For bulk electrical conductivity determination with the spectral induced polarization method (Fehr, 2007; Vanhala and Soininen, 1995), an undisturbed sample is fixed between to electrodes which give an electrical impulse. The electric tension is measured in between the two electrodes M and N and this is used to calculate the specific resistance. The calibration constant is derived from a measurement of a known material (water).

3.2 Results of sample investigation for borehole WW201216

All samples (Table 2, pictures of the core sections are found in Appendix 09) are mainly composed of quartz and feldspar. In addition, minor components as zeolites and carbonates could be identified. In contrast to the other samples the S-72 in a depth of 248.67 m bgl contains more carbonates and some pyrite (detected by DTA-MS). Samples S-73 (249.0 m bgl) and S-81 (265.78 m bgl) were measured in a second lag, both samples mainly contain quartz and feldspar. S-73 stands in contrast to the nearby lower sample S-72 which contains also carbonate and clay minerals (3630er, see below).

Table 2: Overview of core sample sections of WW201216, naming and sample depth. The full sample name consists of borehole number (WW201216), sampling campaign number (1), number of box where core is stored and number of sub sample. Samples were divided into sub samples and hence depth information might vary for the table and the text. A more detailed table is found in the database, see also Appendix 09.

Borehole	Sampling Campaign	Box number S-	Number of sub-samples	Depth from [m]	Depth to [m]
WW201216	1	19	I-IV	126.90	127.25
WW201216	1	22	I-V	136.70	137.17
WW201216	1	28	I-V	153.80	154.23
WW201216	1	45	I-V	201.26	201.76
WW201216	1	52	I-V	218.45	218.85
WW201216	1	54	I-V	219.52	219.91
WW201216	1	72	I-V	248.50	249.00
WW201216	1	73	I-V	249.00	246.45
WW201216	1	81	I-V	265.65	266.13

However, all samples show a broad XRD intensity between 10 - 14 Å and an IR band at 3630 cm-1 which are both indicative of smectite and/or illite. The CEC data indicates the presence of approximately 20 wt. % smectite in samples S-45, S-52, and S-54. For a more detailed characterization of the clay minerals of these samples the < 2 µm fraction has to be investigated. The XRF data, however, does not provide any indication for unusual composition of the clay minerals, as e.g. detected in case of the sample from > 400 m bgl, which was taken from the drill head (chapter 3.5.2).

The low contents of the < 63 µm fraction of these samples which was determined by sieving indicates that the clay minerals are arranged as stable aggregates which, prior to the separation of the clay fraction, would have to be destroyed.

The porosity of the smectite rich samples is only slightly lower than the porosity of the other samples. In this respect it is important to note that the porosity is determined in the dried state in which the swelling clay minerals collapse which in turn creates some porosity not being present in the natural, probably water saturated state.

SEM investigations prove that the smectites (of the smectite containing samples) are situated in the interparticle pores of the quartz grains. In some instances the typical structures of an evaporated smectite gel can be observed (Figure 5).

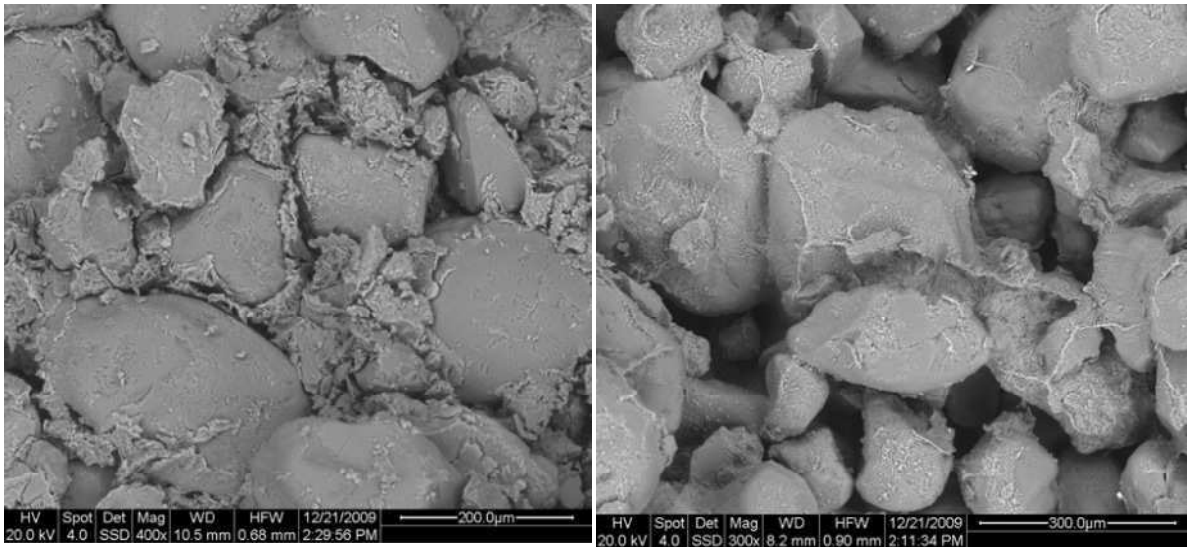

Figure 5: Left: massive smectite aggregates in the quartz-interparticle space, right: smectite threads crossing the quartz grains (typically the result of an evaporated soft smectite gel).

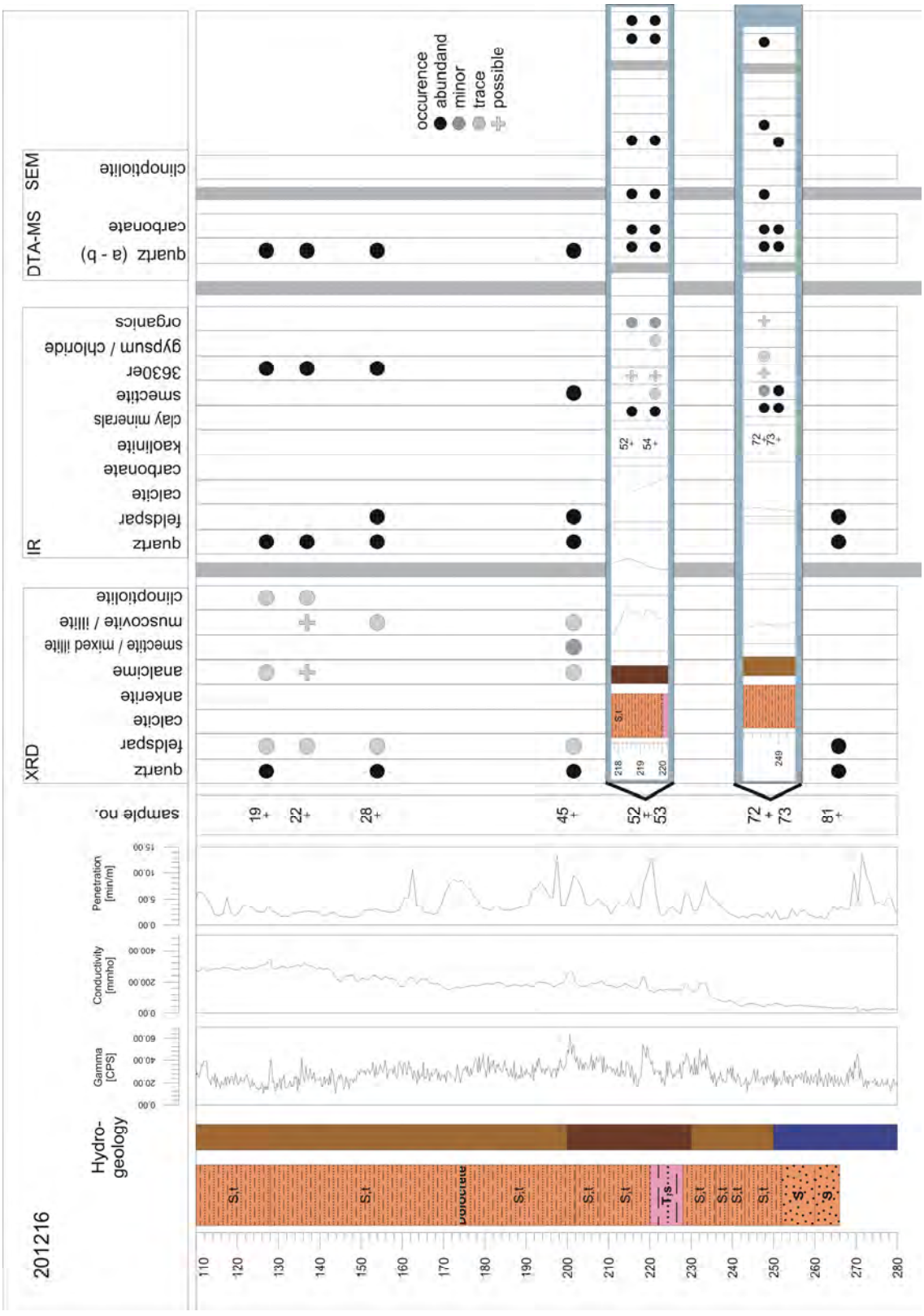

Figure 6: Qualitative mineralogical content determined with different methods: X-ray diffractometry (XRD), Infrared Spectroscopy (IR), Thermoanalytical investigation with a DTA-MS and checking of grains with the Scanning Electron Microscope. Close-up for samples in a depth of 220 m. Litholog from (Miller, 2010), hydrogeology, geophysical logs and penetration from borehole WW201045.

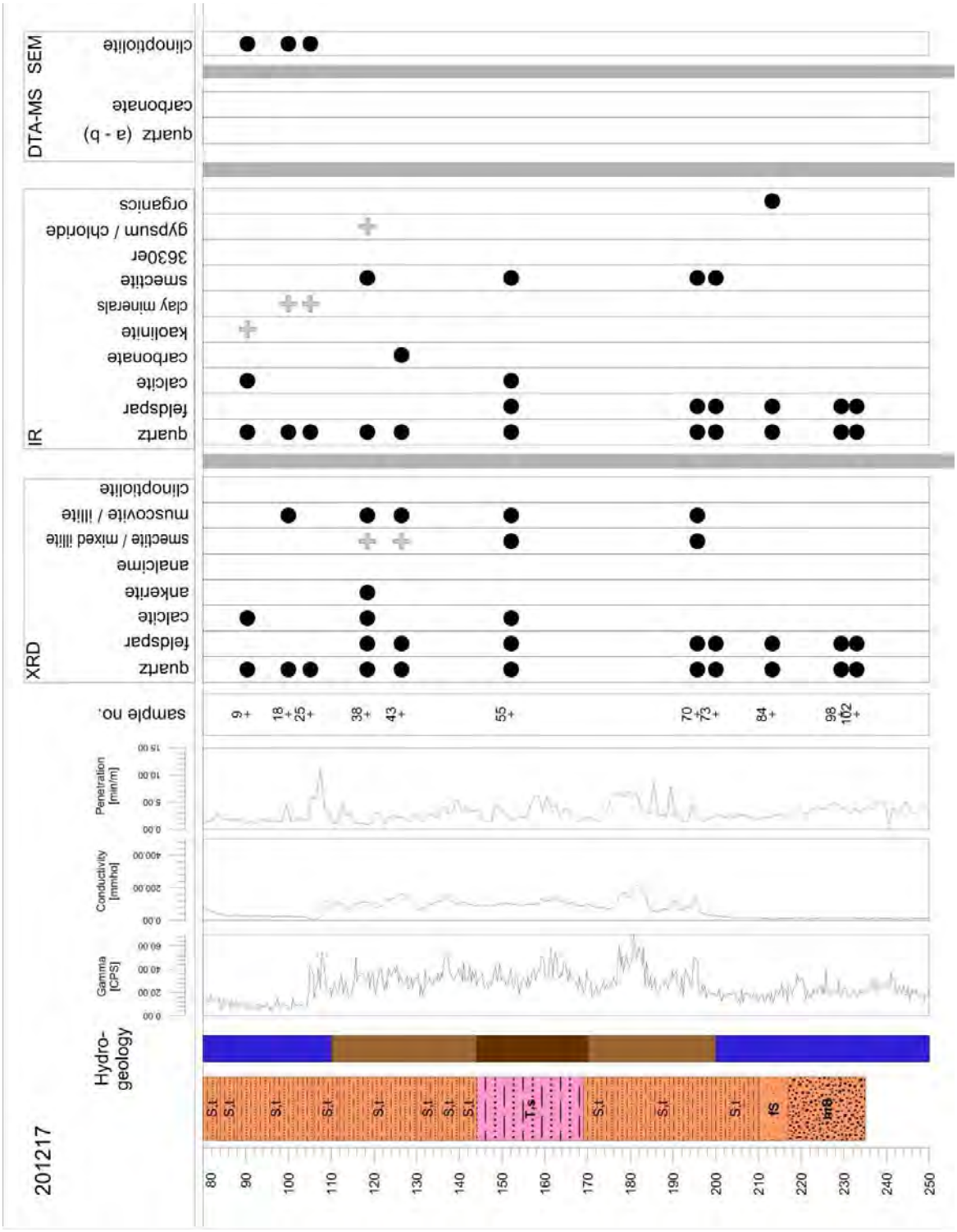

Figure 7: Qualitative mineralogical content determined with different methods: X-ray diffractometry (XRD), Infrared Spectroscopy (IR), Thermoanalytical investigation with a DTA-MS and checking of grains with the Scanning Electron Microscope. Close up for samples in a depth of 220 m. Litholog is from (Miller, 2010), hydrogeology, geophysical logs and penetration are from borehole WW201047.

3.3 Results of sample investigation for borehole WW201217

Eleven samples of WW201217 were shipped to BGR (Table 3), one sample was only partly included into the mineralogical and chemical investigation due to a total disintegration (S-102).

Cation exchange capacity (CEC) and mineralogy: The samples of cored borehole WW201217 can be subdivided into three units. The central unit contains approximately 10 wt. % smectite (as deduced from the CEC). Both the upper and lower unit contains much less swelling clay minerals. In the upper unit traces of well crystallized clinoptilolite could be observed which could not be detected in the lower unit (see ESEM results in the Appendix 10). The distance of the locations of drill holes WW201216 and WW201217 is relatively small. Therefore, it is reasonable to compare the mineralogical results of both drill holes e.g. by considering the CEC which is regarded as optimum mineralogical indicator directly reflecting the smectite abundance (Table 4).

Table 3: Overview of core sample sections of WW201217, naming and sample depth. The full sample name consists of borehole number (201217), sampling campaign number (1), number of box where core is stored and numbers of sub sample. Samples were divided into sub samples and hence depth information might vary for the table and the text. A more detailed table is found in the database, see also Appendix 09.

Borehole	Sampling Campaign	Box number S-	Number of sub-samples	Depth from [m]	Depth to [m]
WW201217	1	9	I-V	89.90	90.40
WW201217	1	18	I-V	99.54	100.00
WW201217	1	25	I-V	105.12	105.58
WW201217	1	38	I-V	117.99	118.50
WW201217	1	43	I-V	126.43	126.77
WW201217	1	55	I-V	151.62	152.18
WW201217	1	70	I-V	195.60	196.11
WW201217	1	73	I-V	199.60	200.08
WW201217	1	84	I-V	213.20	213.70
WW201217	1	98	I-V	228.50	229.43
WW201217	1	102	I	233.00	233.50

The available sample set of both drill holes does not allow for a complete comparison. Nevertheless, some significant differences were observed. As an example, the CEC of the WW201216 in 200 – 220 m bgl is much larger (≈ 20 meq/100g) compared to WW201217. Moreover, such high values were not observed for any sample of cored borehole WW201217. A detailed meaningful interpretation of both sets of values is only possible if both drill holes can be correlated using the geophysical logging-data.

Table 4: Comparison of the CEC (and porosity) of drill holes WW201216 and WW201217 changed from Kaufhold and Dohrmann (2010).

Depth [m]	201216 *Depth [m]*	CEC [meq/100g]	porosity [%]	201217 *Depth [m]*	CEC [meq/100g]	porosity [%]
80						
90				*90*	0.3	32.1
100				*100*	0.1	30.9
110				*105*	0	31.6
120				*119*	8.6	31.9
130	*127*	3.8	30.2	*126*	7.5	28.9
140	*137*	15.8	25.7			
150	*154*	7.5	29.0	*152*	11.2	24.6
160						
170						
180						
190				*196*	12.5	28.7
200	*202*	21.2	23.5	*200*	1.6	41.7
210	*219*	20.6	20.7	*213*	0.0	/
220	*220*	20.4	24.3			
230				*229*	0.5	/
				233	0.3	/
240						
250	*248*	2.8	34.6			
	249	3.5	35.9			
260	*266*	0.8	35.4			
270						
280						

Porosity and microstructure: The total porosity (Table 4, Appendix 10) was determined by measuring the bulk and specific density of the samples and hence reflects the porosity determined by the accessibility of the He atom compared to the so called “dry flow” particles (lower diameter 50 µm). In some of the ESEM images in the appendix the small dry flow particles (≈ 50 µm) can be observed in similar sized pores (Appendix 10).

Measuring the bulk density with the “dry flow” requires the production of stable granules commonly by dry sieving. However, some samples disintegrated upon dry sieving and hence could not be used for measuring the total porosity. Studying the microstructure of these samples by ESEM was also not possible.

All samples consist of well rounded sand sized quartz grains. The swelling clay minerals of the central unit are located in the interparticle space (interparticle pores) and occur as coatings on the quartz grains. From these optical observations it was expected that the CEC and the porosity are related which is proved by Figure 8. Interestingly, both cored boreholes show the same trend and by chance exactly the same regression curve.

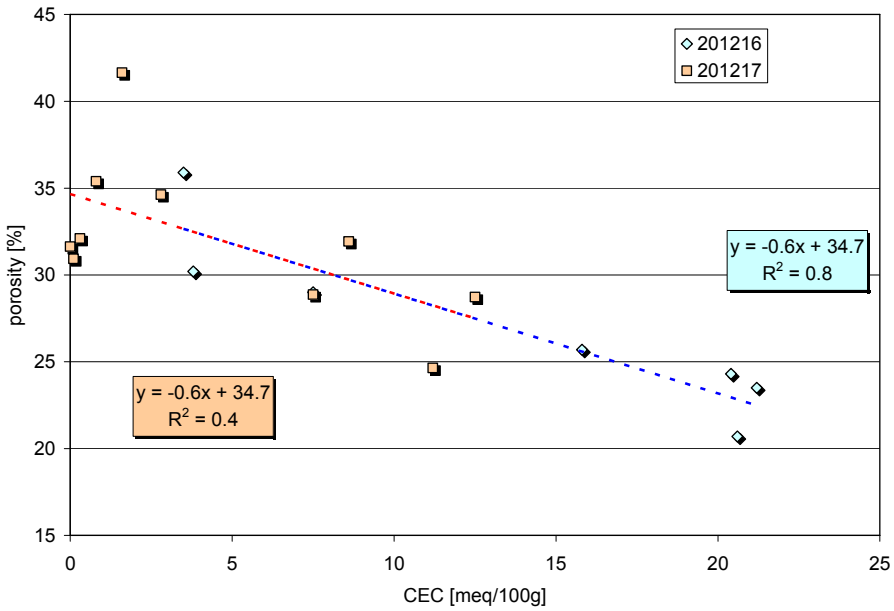

Figure 8: Comparison of the CEC and the total porosity of both cored boreholes.

Interestingly the porosity is significantly larger than one would expect from the low hydraulic conductivity values determined on comparable material (Walzer, 2010), see Chapter 6.3 of Report Part A. Probably this can be explained by the smectites which in the water saturated state swell and form gels of different density. CEC measurements of borehole WW201216 proved the dominance of exchangeable Na over Ca and Mg which results in “free swelling smectites” which typically form low density gels (soft gels) upon water saturation. Even the low density gels are able to seal the interparticle space and which may have significantly reduced the hydraulic conductivity of the rocks. Therefore, the value of measuring the porosity at least in the dry state is questionable. Of course, this porosity cannot be used to calculate any material property in the water saturated state.

Additional observations:

- Clinoptilolite: The occurrence of clinoptilolite only in the upper unit possibly indicates a different milieu throughout sedimentation of the sediments of the upper and the lower unit. Clinoptilolite can form from the same parent material as montmorillonites but is commonly believed to mainly form in highly saline solutions.
- Smectite morphology: Within the smectite containing unit the smectites show different morphology possibly indicating different parent material or different milieu throughout devitrification / smectitisation of volcanic ashes. Parts of the clay fraction have supposedly a volcanic origin and might be volcanic ashes.

3.4 Age determination of duricrusts remnants

Duricrusts are chemical residues caused by pedogenic processes and fluctuating groundwater levels in sediments laid down mainly under tropical climatic conditions. Evapotranspiration and changing redox conditions have a fundamental impact on their precipitation and render these calcareous and siliceous encrustations a valuable marker for the climatic regime throughout deposition of the Kalahari Sediments of Cenozoic age.

Calcareous materials of the 19 core samples were selected separately and sent to an isotope laboratory at the University of Heidelberg for radio-isotope analyses. The chemical composition proved these samples to be unsuitable to determine the isotopic age of the calcareous duricrusts which have only low contents of U and Th. Consequently, we discontinued working in this way and shifted our attention to other isotopes and mineralogical methods to constrain the age of formation – see Dill et al. (2012).

3.5 Results of sample investigation for borehole WW201045

Two sample sets were taken during the rotary drilling, 66 samples from cutting material were taken as well as 1 sample from material that stuck at the drill head which corresponds to the lowest geological layer that was encountered. This clay layer supposedly belongs to a pre-Kalahari formation, e.g. weathered Karoo could have been encountered but this needs further verification.

3.5.1 Grain size and XRF analysis of cutting samples

The grain size distribution for 66 cutting samples was conducted with sieves and a Sedigraph for particles < 63 μm. Class borders for the grain size distribution are <2; 6.3; 20; 63 μm for clay and silt fraction; 63; 112; 200; 355; 630; 1120 and 2000 μm for the sand fraction. In Figure 9, box plots for the three main compartments of the borehole profile of WW201045 are plotted: the overburden from 0 to 80 m bgl, the confining layer from 80 to 240 m bgl and the aquifer from a depth of 240 to 375 m bgl. Below that, from a depth of 275 to 390 m bgl, a layer with slightly lower grain sizes is encountered; these samples were excluded for the box plot graphs.

The plots show that differences are not so significant in between the three main compartments, but clay grain size content is slightly higher in the confining layer and that the coarse sand grain size is higher in the aquifer. An outlier is sample 50 in a depth of 268 m. High carbonate content indicates that a calcrete nodule or layer was likely encountered (Figure 10), which could also counts for the large grain size content. In this stretch (250 – 300 m bgl) only sample 50 was retrieved, why denser sampling was not possible there is not clear. Of course, the grain size samples can only give a trend as they

might be depleted by fine grain sizes due to the washing of samples and suspension of clay minerals during drilling. Also, fine sand components might contain some part of clay aggregates as the material was not disintegrated to a larger extent before sieving. Figure 10 gives an overview of grain size distribution as a log, grain sizes are comprised into clay, silt, fine, medium and coarse sand. Principally, grain sizes seem to be helpful in determining different layers.

The XRF analysis (Figure 10, Appendix 10) shows general trends in the borehole log, it is clear that thin, specific layers are not represented due to the characteristic of the cutting samples of a rotary drilled borehole and that these samples rather give a general picture of sedimentation units. From 0 – 250 m bgl the silica content decreases, at the same time the Al and Na + K content increases showing a link to an increasing amount of clay minerals. The Na + K content increases stepwise in depths of 90 and 200 m bgl, before lower values are encountered again. The Fe_2O_3 log shows an increasing step at 200 m indicating an increased clay content as it is also seen in the gamma log. Generally, the Fe content is low, which means that magnetic susceptibility measurements as were conducted in borehole WW201045 twice must show only slight changes. Borehole logging campaign II resulted in an area of magnetic activity in a depth of 200 to 240 m bgl, which corresponds with the measured slightly elevated Fe_2O_3 content there (Appendix 10.4). The sensibility of the magnetic susceptibility device was not strong enough to detect other major magnetic signals.

Chemical results of Sample 50, in a depth of 268 m bgl, show a distinct different characteristic which is probably due to a calcrete nodule within the sample. From a depth of 300 – 370 m, high silica indicates low clay content. From a depth of 375 to 390 m bgl, the clay content increases again. Laboratory results of the lowest material encountered (see sample discussion next chapter), is included into the logs, which was derived from the clay sample sticking to the drill head. It should be noted that this belongs to another sampling method but at the same time shows very a different characteristic to cutting samples (Figure 10). Nevertheless an increase in clay mineral content is also seen in the main and trace element distribution already beforehand from a depth of 375 m bgl.

Arsenic (As) content clearly fluctuates and has higher values from 0 – 75 m bgl and again from 160 – 200 m bgl. Co, Nb and Y show some exceptional peaks but all other elements show no distinct pattern. An exception is Copper (Cu): the uppermost 26 meters show an elevated content, it seems that aeolian sands that are identified in more shallow boreholes (Wyk, 2009b) are encountered here and are distinguishable from the other sediments. All plots of trace elements are found in Appendix 10.4.

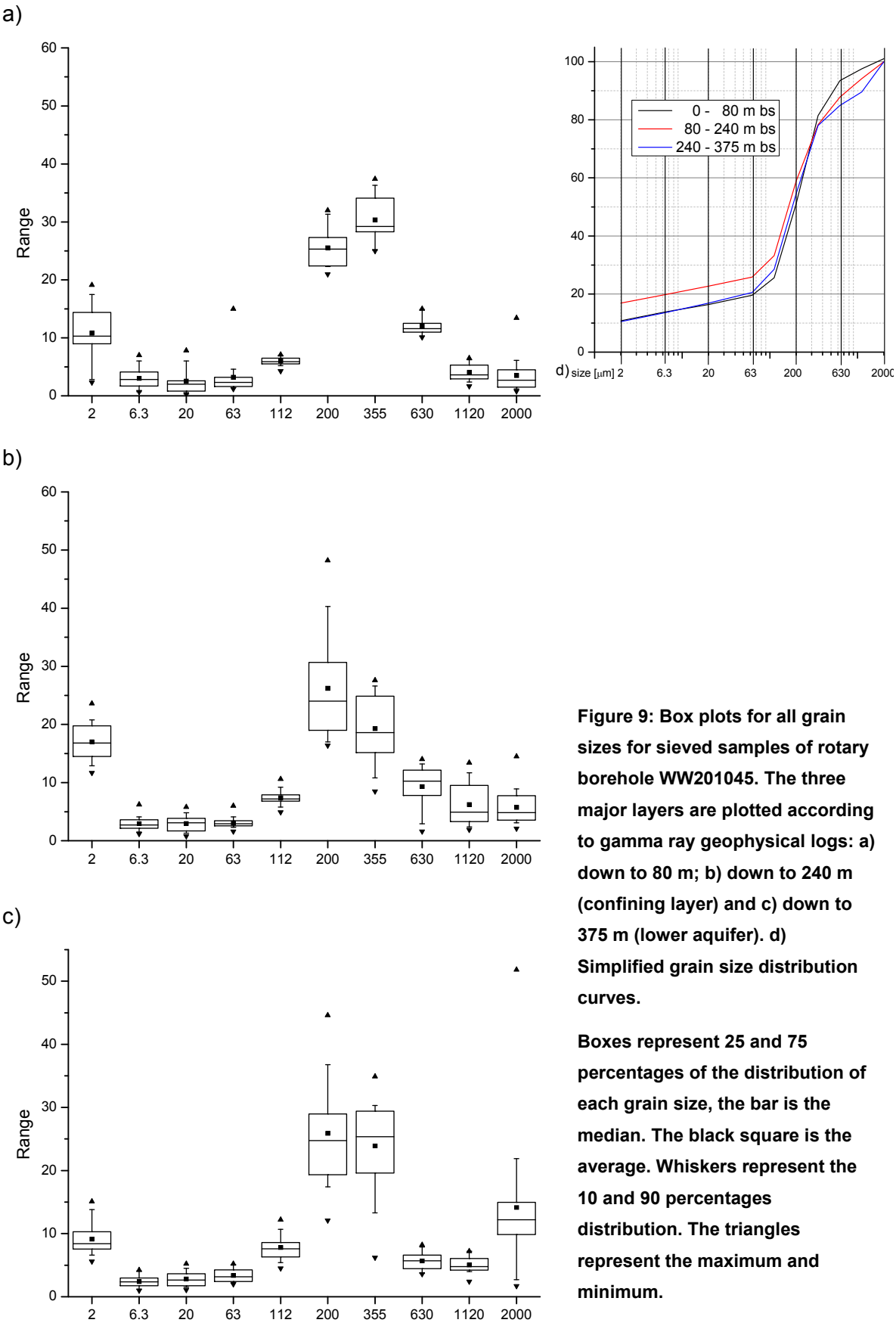

Figure 9: Box plots for all grain sizes for sieved samples of rotary borehole WW201045. The three major layers are plotted according to gamma ray geophysical logs: a) down to 80 m; b) down to 240 m (confining layer) and c) down to 375 m (lower aquifer). d) Simplified grain size distribution curves.

Boxes represent 25 and 75 percentages of the distribution of each grain size, the bar is the median. The black square is the average. Whiskers represent the 10 and 90 percentages distribution. The triangles represent the maximum and minimum.

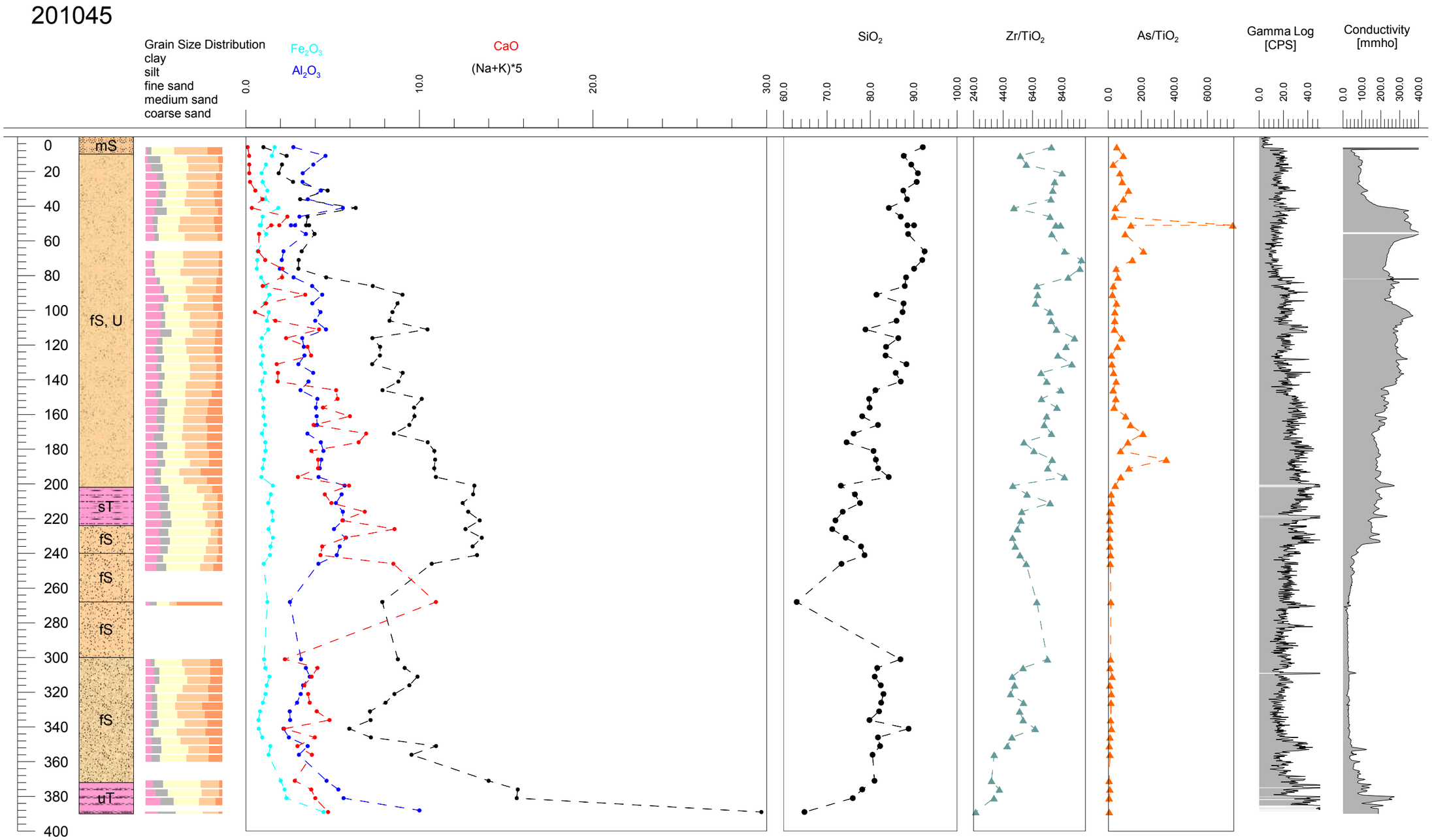

Figure 10: Grain size distribution for sieved samples and some of the element content of the XRF Determination of rotary borehole WW201045 (66 samples).

3.5.2 Clay sample of lower most layer

About 10 g air dried material was provided for this analysis; it was dried at 60°C, and ground by a mortar mill. For ESEM investigation a small entire piece was separated.

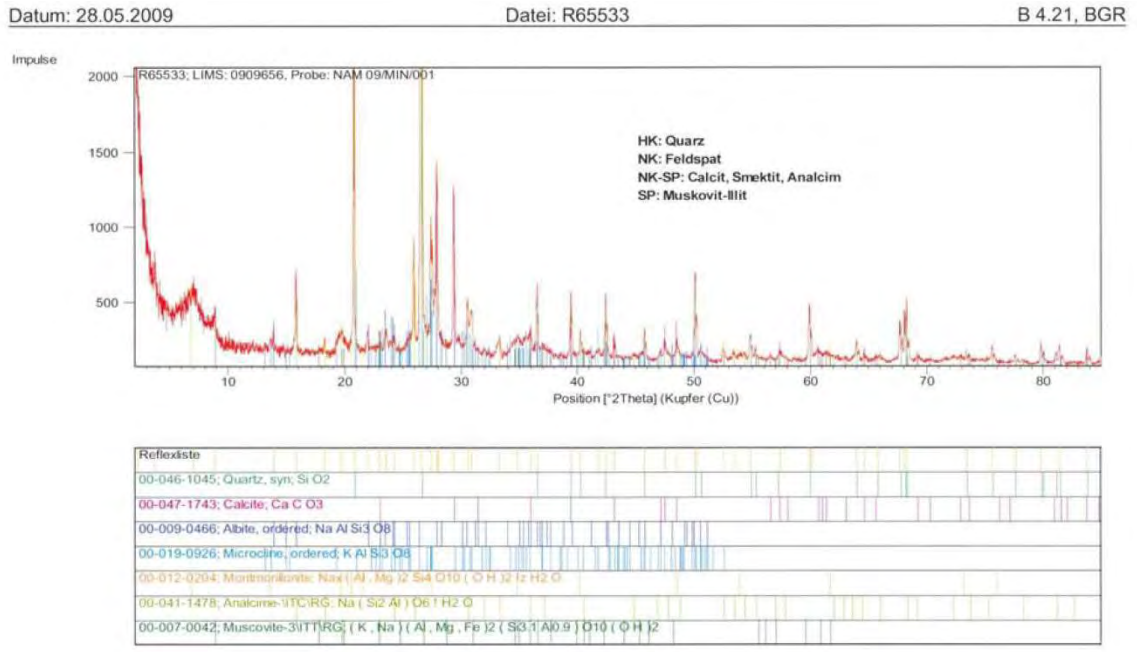

Figure 11: XRD pattern of the clay sample of the lowest layer.

The XRD pattern of the bulk material shows a broad but pronounced smectite reflection. Considering the symmetry of this reflection suggests that illite/muscovite and smectite are present as separate phases, but this has to be investigated in more detail (by investigation of the clay fraction). Next to feldspar, calcite, and quartz, some analcime was found.

The XRF analysis revealed that the most striking feature of the chemical composition is the high MgO content which commonly indicates the presence of dolomite and/or magnesite. Considering the mineralogical composition, however, suggests that the smectite mineral is the only Mg bearing phase. The concentration of the other main elements does not attract attention in contrast to the high Cu content, which probably provides information about the source rock of the clayey material.

The CEC accounts for 20 meq/100 g and the sum of exchanged cations exceeds this value by far which is a common observation in case of calcite as minor component. Therefore, the exchangeable Na^+, being in good agreement with the T-value, is supposed to represent the only exchangeable cation. In conclusion it has to be assumed that the smectite occurs in its Na-form which is i) rare and ii) interesting with respect to the swelling and in turn hydraulic properties.

By ESEM no preferred orientation could be observed (which is characteristic of sedimentary materials). With larger magnification the coating of the coarse minerals by smectites can be seen.

The IR band at 3680 cm^{-1} provides some indication for the existence of trioctahedral minerals in the sample, possibly saponite, which would explain the high MgO content. The OH-bending region, unfortunately, cannot be interpreted owing to the dominance of the carbonate.

The clay fraction of the sample is about 35 %. Assuming a smectite content of about 20 wt. % suggests that other minor constituents are present in the < 2 µm fraction.

Using both the qualitative mineralogical composition (assuming the presence of saponite) and the chemical composition a rough estimate of the quantitative mineralogical analysis can be calculated.

The investigated sample shows some features which are not typical of “normal” sedimentary clays: i) high MgO content (=presence of saponite being a fairly rare smectite), ii) presence of analcime, iii) absence of any preferred orientation, iv) high Cu content, and v) Na^+ population of smectite interlayer. All parameters suggest that at least the smectite is derived from the alteration of mafic rocks. The Cu content possibly helps to identify the source of the material.

3.6 Comparison of bulk rock electrical conductivity and fluid conductivity

In Figure 12, the bulk rock electrical conductivity (EC) is plotted parallel to the fluid conductivity (FC) calculated from results of the elution method (EC from the 1:10 elution). A high bulk rock electrical conductivity and low fluid conductivity show areas where clay content prevails and fluids are considered to be fresh water. The comparison of these methods with the gamma and conductivity logs helps to determine these signals. Conductivity increases with increasing clay content but also with increasing salinity of pore fluids. Element distribution of the eluates, representing pore fluid content is listed in Appendix 10.8. These will be further investigated with the additional samples that are currently investigated. It is noteworthy that some samples show high SiO_2 contents, which might be an indicator for smectite building fluids.

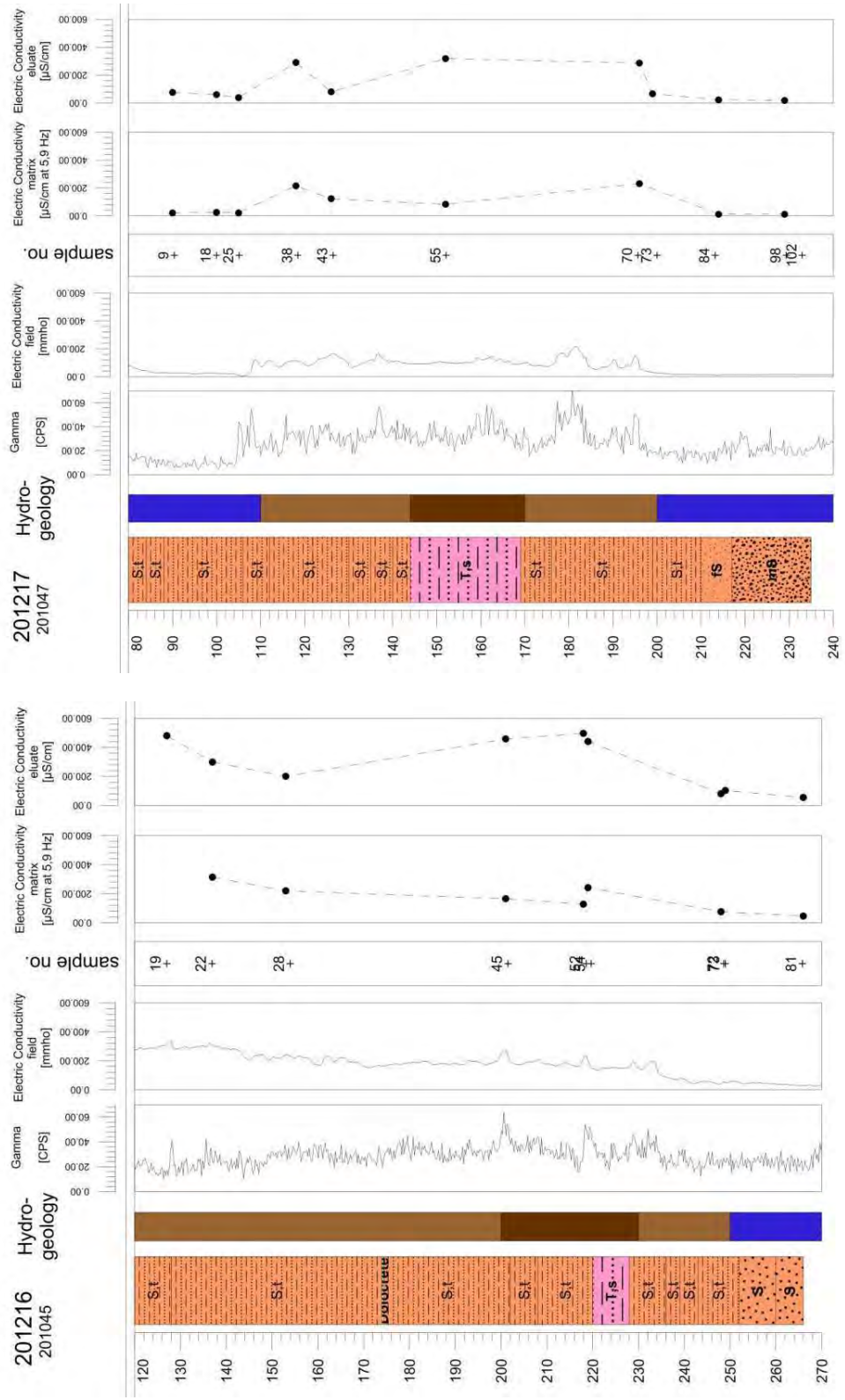

Figure 12: Values of electrical conductivity of the geophysical borehole logs of boreholes WW201045 and WW201047 compared with core sample analysis for bulk and fluid conductivity from cored boreholes WW201216 and WW201217.

4 Micropaleontology

By Juliane Fenner

In this chapter the results from analyses of changes in the abundance and preservation of biosiliceous component groups and taxa in the silt fraction are presented. The goal of this investigation was a) to test which paleo-environmental information and b) which age information can be provided from theses analyses deltaic sediments in the Cubango Megafan.

In order to evaluate the intensity of silica diagenesis, authigenic zeolites were included in the analysis. These hydrous siliceous minerals are generally silt-sized and form authigenically from mobilized silica in the pore water. Under alkaline conditions e.g. this diagenetic process is speeded up. In addition, the abundance of the silt fraction as well as the clay fraction was determined.

4.1 Methods

From the two cored boreholes, WW201216 and WW201217 (for location see Figure 1), selected sections of 20 – 60 cm length had been brought to the BGR by Walzer (2010). Of these core sections 26 subsamples were chosen for this study, which concentrates on the biosiliceous components and zeolites in the silt fraction.

The preparation methods had the goal to concentrate:

- Diatoms and other biosiliceous remains of aquatic organisms,
- Siliceous remains from land plants, mainly opal-phytoliths from these delta deposits dominated by minerogen detritus.

In samples from depths WW201216-52-1-I, 218.45 – 218.56 m bgl and WW201216-72-1-V, 248.84 - 248.85 m bgl the size of the calcretes was large enough to warrant the possibility of a separate analysis of these calcretes for siliceous microfossils. This was done to test whether siliceous shelled microfossils had been preserved in these concretions, and if yes whether their preservation differed from that of the surrounding sediment, thus getting information how early during diagenesis these concretions had formed.

The following preparation steps and methods were applied:

1. After separation from the sand fraction and clay fraction, using sieving and the Atterberg method, the remaining silt fraction of each dried and weighed sample

was boiled in a mixture of 40% acetic acid and 30% H_2O_2 in order to dissolve carbonates and oxidize fluffy organic matter,

2. Quantitative slides had been prepared following the method of Battarbee (1973) and using Zrax (n.d. 1.7) as embedding resin,

3. Further concentration for siliceous microfossil groups was achieved by heavy liquid separation using a solution of sodiumpolywolframate with a density of 2.3, non-quantitative slides were prepared from this concentrate,

4. Relative abundances of biosiliceous components and zeolites in the silt fraction were determined using a light microscope Leitz Axioplan 2 at a magnification of 400 times. Quantitative counts will be made when more and closer spaced samples are available.

5. Scanning electron microscopes (SEM) were used: for taxonomic determination of the diatoms, to resolve and document the fine structures of their valves, and - in order to document phytolith types and authigenic minerals in the silt fraction, a) platinum/paladium-coated non-quantitative slides of the preparation residue after boiling in acetic acid and H_2O_2 and washing out the surplus acid afterwards were checked using a FEI Sirion 200 at a voltage of 5kV. b) non-sputtered silt-sized particles, which were not chemically treated, were checked in a FEI Quanta 600 F operated at low vacuum (0.6 mbar), at a voltage of 20 kV, and in BSE mode (backscattered electrons).

It was tested, whether the depths of clay peaks in the cored boreholes correlated with peaks in the natural gamma curve of the logged boreholes in order to overcome the problem how to correlate the results from samples of the cored but not logged boreholes WW201216 and WW201217 to the natural gamma curves of the nearby boreholes WW201045 and WW201047, which were logged. For this purpose, the percentage of clay and silt in some of the samples was determined (Figure 13). For the grain size analysis of other samples and the sand fraction see chapter 3 (Kaufhold and Dohrmann, 2009a; Kaufhold and Dohrmann, 2010).

Sedimentological subsamples: For 8 samples, the following preparation steps were followed for zeolite identification and in order to determine the weight percent of the silt fraction and of the clay fraction:

1. drying at 40°C + determining the dry weight of the sample,

2. dry sieving the sediment through 63 µm + determining the dry weight of the sand fraction.
3. Siphoning off of the clay fraction using the Atterberg method and sodium hexametaphosphate to help suspending the clay. The time to siphon the clay off, after suspension of the sediment in the beaker, was calculated using Stokes law. This procedure was performed as long as there was still suspension to be siphoned off, at least six times,
4. wet sieving the silt fraction through 20 µm and determining the dry weight of the fractions 2 - 20 µm, 20 - 63 µm,
5. Zeolite identification was done by shape in the light microscope and SEM as well as with EDAX and XRF.

4.2 Results

4.2.1 Grain size analysis

The determination in 8 samples of the amount of the silt fraction and the clay fraction of the sediment shows that:

1. the grain size of the sediment varies dramatically (Table 5).
2. There is a general trend through the clay-rich core interval of up-section decreasing clay fraction and increasing sand fraction, which is correlated with decreasing values in the natural gamma curve (Figure 13).
3. Of the 8 test samples one has sampled an interval with high clay contents: WW201217, 195.6 m with 88,6 % clay. This sample correlates in depth with the highest gamma peak in WW201047 (Figure 13).
4. Points 2 and 3 mean that first; the natural gamma curve reflects mainly the abundance of clay minerals in the sediment. And secondly the grain size analysis (abundance of the clay fraction) can be used for correlating the cored but not logged cores with the logged boreholes.

In Figure 13 the gamma profiles of WW201045 and WW201047 are arranged so that the clay-rich interval of both boreholes correlates and the grain size results from the few test samples of boreholes WW201216 and WW201217 are plotted following the depth scales of WW201045 and of WW201047 respectively. This procedure can be justified by the findings that in all boreholes the sequence of sedimentary units seems to be the same,

and that the trend in the microfossil contents of the two cored boreholes agree, as do also the natural gamma profiles of the two logged boreholes.

Table 5: Grain size analysis of 8 selected samples.

		sand	silt		clay
depth from [m]	depth to [m]	>63 µm	20-63 µm	2-20 µm	< 2 µm
WW201216					
136.97	136.99	69.7	4.1	1.3	24.8
154.07		72.5	4.5	3.2	20.0
201.53		64.2	7.2	4.6	24.1
219.52	219.6	45.8	3.4	4.4	46.6
219.67	219.83	40.4	2.9	3.5	53.3
248.82	248.83	87.7	2.5	0.6	9.2
WW201217					
90.27	90.29	87.45	4.2	3.1	4.7
195.6		5.2	1.4	4.7	88.6

Microscopic analysis of the silt fraction shows that the coarse silt fraction (20-63 µm) generally is dominated by detrital grains (quartz with ca. 1% of it ironoxide-stained, orthoclase, plagioclase, albite, micas, and very subordinate heavy minerals) together with fragments of chert, zeolites (like clinoptilolite, analcime) being less abundant. In the fine silt fraction often the authigenic zeolites are the dominant component, and among the detrital minerals the heavy minerals are more prominent, like zircon, titanite, andalusite.

4.2.2 Relative abundance of siliceous microfossils

In sands, the abundance of siliceous microfossils generally is very low. One reason is often the high sedimentation rate of sands resulting in dilution of other particles. Another reason for the low preservation potential of siliceous microfossils is the often high percentage of open pore space in sands, which often is filled with pore water that is under-saturated by silica. In moving sands in addition mechanical destruction of biosiliceous particles plays a role. Because if any, only low amounts of biosiliceous particles could be expected, the above described extensive concentration techniques were applied.

In all samples analyzed of cores WW201216 and WW201217 siliceous microfossils were encountered (Table 6), thus from samples from within the clay-rich interval as well as from samples from the sands above and below it.

Present are siliceous remains from land plants (phytoliths) and also siliceous remains of aquatic living organisms: algae (valves of benthic, planktonic and tychoplanktonic living diatoms and resting spores of *Chrysophyceae*) and spicules of sponges. The most abundant group among the siliceous microfossils is the opal phytoliths of grasses.

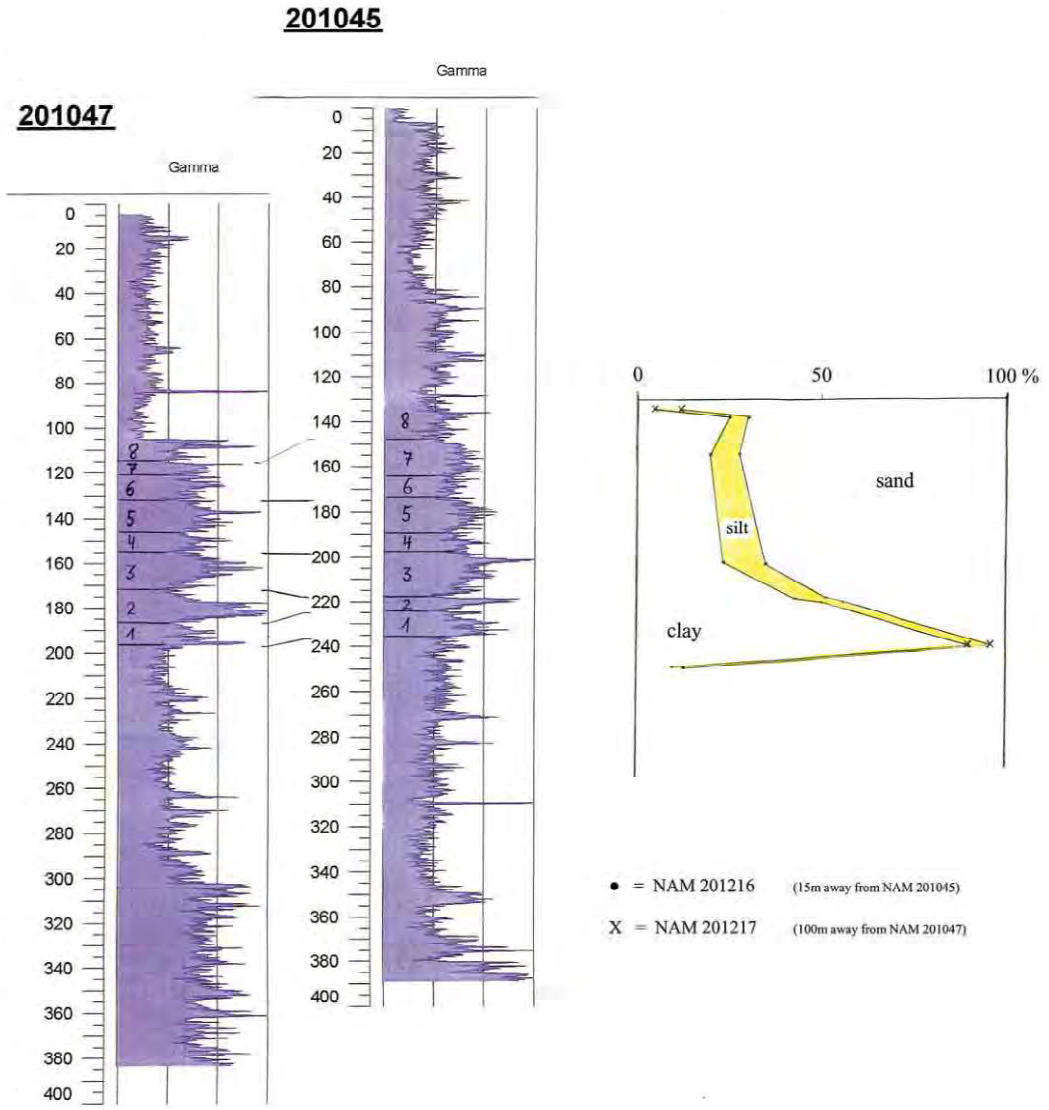

Figure 13: Abundance of silt-size particles in a few test samples of cores WW201216 and WW201217 plotted against the depth and logs of natural gamma radiation of the close by boreholes WW201045 and WW201047. The two logs have been correlated based on the similarity of cyclicity observed in the clay-rich interval.

The pattern of occurrence of the siliceous microfossils (Figure 14 and Figure 15), is the same in both cores. In most samples the abundance of biosiliceous components is very low, but at the same position in the sedimentary sequence their abundance is generally slightly higher in WW201217 than in WW201216. While opal phytoliths are present in all samples, siliceous remains of aquatic living organisms are absent to extremely rare in the few samples from the central part of the clay-rich interval of both cores. The only samples richer in all siliceous microfossil groups are the samples from the uppermost part of the clay-rich interval in core WW201217.

Concerning the siliceous microfossil content in calcrete samples of the test samples there is no significant difference, neither in the abundance and preservation of diatoms, sponge spicules, and phytoliths nor in the content of authigenic minerals between the two calcrete samples and the matrix sediment.

In the following the results are presented by siliceous microfossil group.

4.2.3 Opal phytoliths

Many plants, e.g., some angiosperms (e.g. *Magnoliaceae*), *pteridophytes* (ferns, tree ferns, horsetails), *monocotyledons* (grasses, sedges, palms, *Bromeliaceae*), eudicots (*Asteraceae, Cucurbitaceae, Ulmaceae*) secrete bodies of amorphous hydrated silica, opal phytoliths, into the vacuoles of cells or into intercellular space. Among the monocotyledonous plants, especially the *Poaceae* are prolific producers of relatively robust and dissolution resistant opal phytoliths. After the plants decay, the dissolution resistant opal phytoliths accumulate in the soil.

Since the revival of interest in opal phytoliths by Baker (1959; 1960) and Twiss et al. (1969) and the demonstration of their usefulness as paleo-environmental indicators by these authors, a multitude of studies has been performed on this fossil group. As a consequence the terminology of opal phytoliths has been refined, and the knowledge on which plants produce which phytoliths has been improved, so that it is much better known now which phytoliths are taxonomically diagnostic. As not all plants produce opal phytoliths, and as those which do, do not do so in equal amounts and equal resistivity to dissolution, and as only few opal phytoliths are species or genus specific, one cannot conclude from the phytolith assemblage back to the floral assemblage. Nevertheless certain types of opal phytoliths are characteristic of certain plant groups and their abundance or ratios calculated from them can be used as paleo-environmental indicators. A multitude of publications is testing their usefulness.

For central Africa (Congo) opal phytoliths have been studied by e.g. Runge (1999), for Namibia by Mulder and Ellis (2000).

Opal phytoliths are present in all samples analyzed of WW201216 and WW201217, and they are the most abundant siliceous microfossil group in these sands. Examples of different types are illustrated on Plate 1 and Plate 2 in Appendix 11.1 and 11.2. All the illustrated specimens are from the sample with the best preservation of biogenic silica.

Among the opal phytoliths those of grasses are dominant. And among the grass opal phytoliths it is the panicoid and chloridoid types of C4-grasses which dominate (Appendix 11.1). The latter are the typical grasses of tropical and subtropical regions with low to

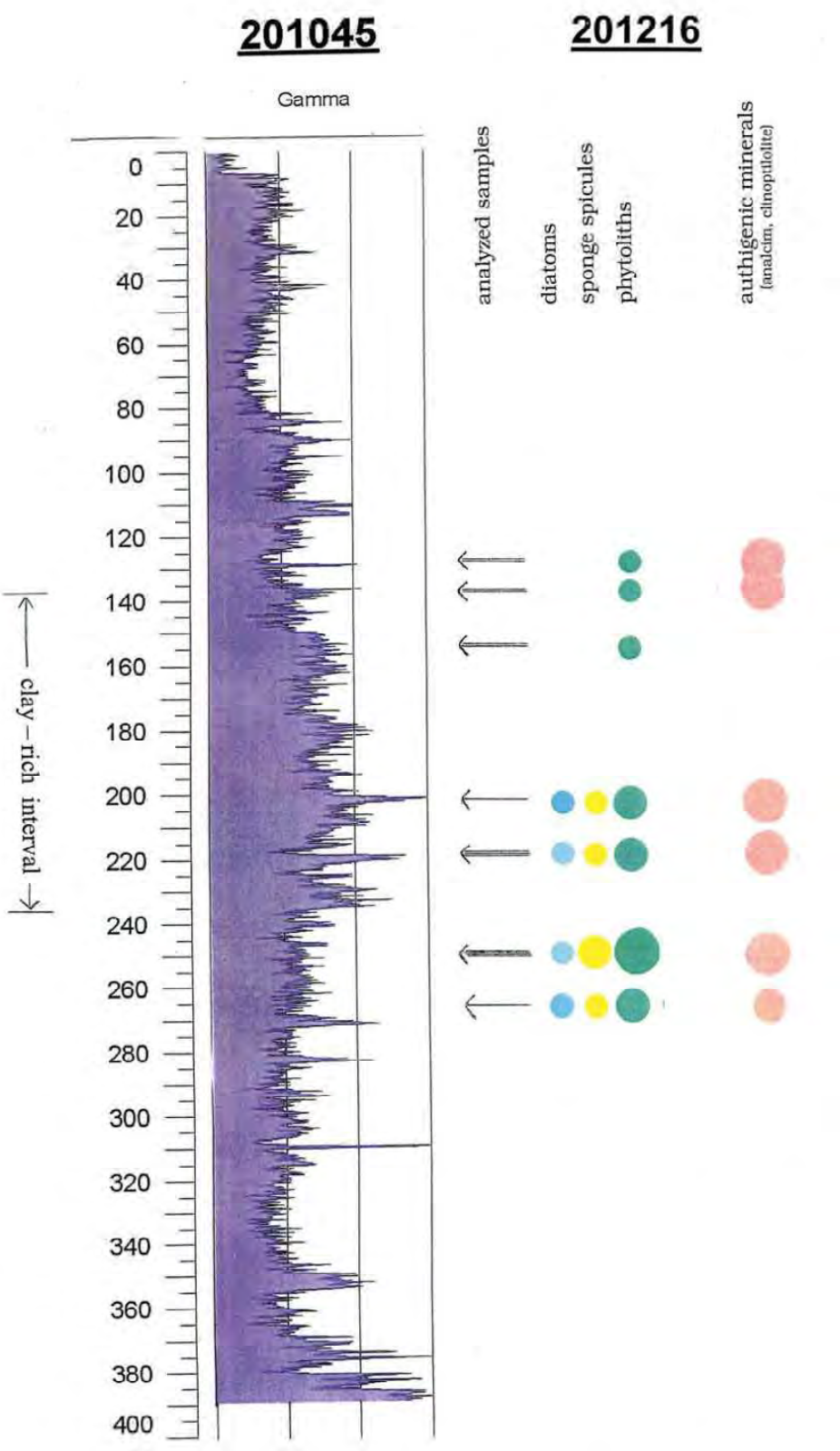

Figure 14: Relative abundance of siliceous microfossils and authigenic minerals (e.g. clinoptilolite, analcime) in test samples from core WW201216. Geophysical logs are from nearby borehole WW201045 (8 m).

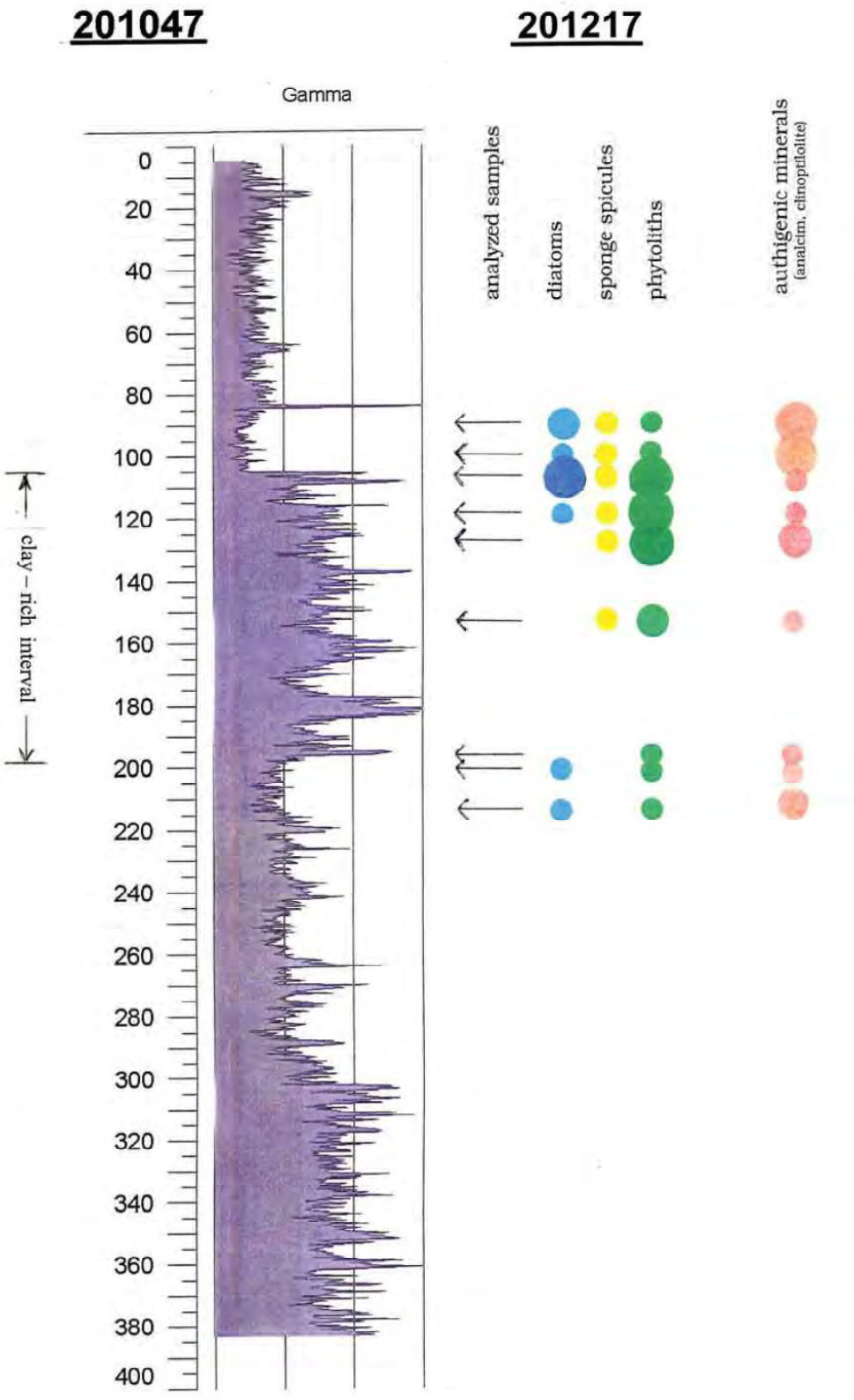

Figure 15: Relative abundance of siliceous microfossils and authigenic minerals (e.g. clinoptilolite, analcime) in test samples from core WW201217. Geophysical logs are from nearby borehole WW201047 (<100 m).

moderate soil moisture. Festucoid fan- and saddle-shaped types (Appendix 11.2e-h) occur more rarely. Opal phytoliths from trees, shrubs, and palms (Appendix 11.2m-n) do occur but remain subordinate to those of grasses.

The dominance of remains of C4-grasses suggests that the age of the deposits lies somewhere in the time interval from middle Miocene to Recent.

Opal phytoliths are more dissolution resistant than diatom valves. One reason for it is that because of their massiveness their surface area is small compared to that of diatom valves. The second reason is that the opal of most phytoliths is less rich in OH-. In sample WW201217, in a depth of 105.05 m bgl in which siliceous microfossils are most abundant and best preserved, besides well preserved opal phytoliths also specimens occur, which show clear dissolution effects (Appendix 11.1 l, m).

Table 6: Relative abundance of siliceous microfossils and plants.

borehole	depth	remains of land plants			remains of aquatic organisms			
		phytoliths		pollen	diatoms		sponge spicules	chrysophyc. resting spores
		grass	tree		planctonic	benthic		
201216	127.09	S						
	127.25							
	136.8	R						
	136.97	R						
	153.95	S	S					
	154.07	S	S					
	201.52	F	R		S		S	
	201.53	F	R				S	
	218.45	R	R					
	218.85	F	R				R	S
	219.5	F	F		S	S		R
	219.52	S	S	S	S			R
	248.5	S	R	S				
	248.68	S	F		S		S	S
	248.84	R	F	S				S
	249.45	C	F		R	R	F	S
	265.77	F	S			S	S	
201217	90.27	R	R		R	F	R	
	99.5	S	R			R		
	105.05	A	F		F	F	R	
	118.38	A			R	S	R	
	126.6	C					R	
	152.1	R	F					
	195.6	R						
	199.77	R		S	S	R		
	213.2	R		S		S		

S = single, R = rare, F = frequent, C = common, A = abundant

4.2.4 Diatoms

Diatoms are unicellular algae, which generally secrete a two-partite, pill-box-like constructed siliceous shell that can be preserved in the sediments. Diatoms are widely

distributed. They live in nearly all aqueous environments on land and in the sea, and there is an incredible number of species. Many of them are highly specialized to survive and thrive in different environments. These characteristics make diatoms good environmental indicators, e.g., for salinity, water chemistry, water depth, paleo-productivity.

In cores WW201216 and WW201217 the abundance of diatom valves and remains thereof is very low. All specimens encountered are of relatively small species. In the central part of the clay-rich interval in both cores no diatoms or fragments of their valves were encountered. Single occurrences are registered in the sands just below and above the clay-rich core interval and in the samples from the lower part of the clay-rich interval. Only in the upper part of the clay-rich core interval in WW201217 the number of diatoms encountered per slide is higher and their preservation is better. All illustrations on Appendix 11.3 therefore have been taken from sample WW201217, at 105.05 m.

Because the diatoms are so few, relatively small, and only part of them was found with complete valves, in most cases their taxonomic determination in these few test samples was possible only to the genus level.

4.2.5 Paleo-environment

From taxonomic determination of the diatom valves on the genus level it is clear that we are dealing in all test samples with remains of freshwater diatoms.

Remains of benthic living diatom species (Appendix 11.3c-f) and of planktonically or tychoplanktonically (species able to adopt a life style either as plankton or as benthos) living diatoms (Appendix 11.3a, b) were found in about equal amounts.

There is only one single find of a valve of a fully planktonically living diatom, the centric genus *Aulacosira*. Because the members of this genus are living planktonically, finds of their valves generally are taken to represent deeper lake water. All other centric diatom specimens encountered belong to three different, small species of the genus *Cyclotella*. The species of this latter genus live planktonically or tychoplanktonically. One *Cyclotella* species could be identified as belonging to the *C. meneghiniana* species group. This species group belongs to the taxa, which Hecky & Kilham (1973) reported as characteristic for weakly alkaline saline lakes in Kenya and Tanzania.

Among the benthic diatoms robust valves of at least two different species of the epiphytic genus *Epithemia* were encountered, as well as fragments of valves of the genus *Cocconeis*, which is epiphytic or epilithic, further fragments of valves of the epipsammic genera *Rhopalodia* and *Surirella*. In addition single pennate species of the genera *Nitzschia*, ?*Navicula*, and *Brachysira* were encountered. These species altogether

suggest a shallow lake environment, but deep and large enough that water persisted for several years and provided a habitat for such water plants.

Although diatoms are rare, there is a slight indication that there are differences in the occurrence of taxa in the two cores: in WW201216 diatoms are rarer than in WW201217. While species of the genus *Cyclotella* and of the benthic genus *Surirella* were encountered in both cores, the only find of a valve of the fully planktonically living diatom *Aulacosira* was found in WW201216. On the other hand the clearly epiphytic species of *Epithemia*, the occurrence of which therefore is coupled to the occurrence of large aquaeous plants, is restricted to WW201217. If this trend proves to be true, this would place WW201216 in a position deeper in the lake and further away from plants growing along the lake fringes than WW201217.

4.2.6 Diatom preservation

Diatom valves are highly perforated (areolae and pores) and posses decorative valve structures, both resulting in a high surface area. These constructional characteristics as well as the relatively high OH^--content of their opal makes them one of the more dissolution susceptible biosiliceous components.

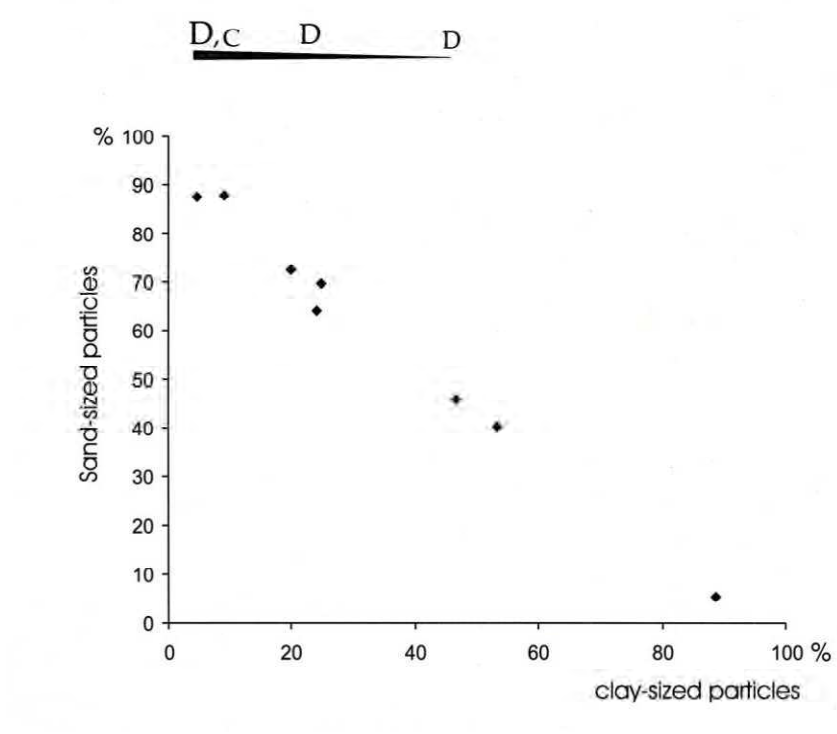

Figure 16: Occurrence of diatoms and chrysophycean cysts in relation to the clay and sand content of the sediment of cores WW201216 and WW201217. D = diatoms present/ preserved; c = chrysophycean cysts present/ preserved

While diatoms generally are better preserved in clays than in sands, here we find an opposite relation. The example of the occurrence of diatoms (Figure 16) shows that diatoms are practically absent at higher clay values (> 50%), and increase in abundance towards a higher percentage of sand. The same is valid for resting spores of chrysophytes, and other siliceous microfossils. This suggests that silica diagenesis in the clays is increased, providing even less preservation potential for biogenic opal.

An amazing finding was the wide spectrum of different preservation stages of the diatom valves in the analyzed samples. Besides strongly etched fragments of robust valves e.g. of the genus *Epithemia* (e.g. Plate 3 in Appendix 11.3a) in the same sample whole, well preserved valves of *Cyclotella* were found as well as poorly preserved *Cyclotella* valves. A possible explanation of such different preservation within one sample is indicated by the observation that in the sediment, which was not boiled in acetic acid and in the oxidant H_2O_2, the one encountered whole valve, which was well preserved, was surrounded by organic matter making photography difficult to impossible. This organic envelope could of course have protected the siliceous shell from dissolution. Another possibility is that, in the relatively large sample prepared and concentrated for diatoms, it is possible that layers of different silica preservation were mixed together.

Another topic that has to be dealt with, when so few diatoms are found, is whether it can be excluded that the encountered diatoms are contamination. Laboratory contamination can be excluded, because those species found are unknown from samples prepared earlier in the same laboratory. Concerning the possibility of contamination from the water used as drilling fluid, A. Walzer informed that water from the close by respective “sister borehole” WW201045 for WW201216 and WW201047 for WW201217 had been used for drilling fluid and not water from e.g. a nearby pond or other surface water. An argument suggesting that we are not dealing with contamination by diatoms imported with the drilling fluid is that the pattern of occurrence of diatoms through the three upper units of the two cores is the same and not a random occurrence as might be expected if they were contamination.

4.2.7 Age

The evolution of freshwater diatoms is not so well studied as that of marine planktonic diatoms. While for the latter a detailed high resolution stratigraphic zonation has been developed for the Cenozoic, for freshwater diatoms only a rough scheme on the evolution of centric Neogene genera exists (Krebs and Bradbury, 1995; Ognjanova-Rumenova, 2000).

The diatoms recovered from the samples of WW201216 and WW201217 are of typical Neogene character. Unfortunately the two centric genera occurring belong to the very long ranging genera *Aulacosira* and *Cyclotella*. Of these, *Cyclotella* narrows the possible age to somewhere younger than Early Miocene, thus younger ca. 16 Ma.

Comparative studies on well dated diatom-containing deposits from lakes and salt pans in Namibia and surrounding countries should be done to obtain a better basis for more accurate age determinations.

4.2.8 Sponge spicules

The occurrence of siliceous spicules of sponges in cores WW201216 and WW201217 is similar to the occurrence of diatom remains, and they are similarly rare. All spicule types occurring in the two cores belong to the monaxons. Monaxons are produced by practically all sponges, marine and freshwater. But siliceous spicules of marine sponges possess a multitude of different spine types, freshwater sponges produce only monaxons and amphidiscs. The simple monaxon types of spicules, occurring in the analyzed samples, suggest that the sediments of the deltaic body were deposited in a lacustrine environment.

Siliceous sponge spicules like opal phytoliths are known to be relatively dissolution resistant. The observed pattern that these two more dissolution resistant components occur further into the central part of the aquitard interval than diatoms (Figure 14 and Figure 15) support the suggestion that this central part of the aquitard core interval is characterized by increased silica dissolution.

4.2.9 Chrysophyte resting spores

Siliceous resting spores (stomatocysts) of chrysophycean algae (classes *Chrysophyceae* and *Synurophyceae*) are hollow globose, oval, bulbous, or pyramidal bodies with a single pore, which is still closed by a lid in unhatched specimens and open in hatched ones. The ornamentation of the outside of the resting spore is a result of genetic as well as environmental factors (Sandgren, 1983). It may be smooth or more or less ornamented by structural elements like ribs, knobs and spines. The pore may or may not be surrounded by a collar. Such chrysophyte resting spores are occurring in the marine and the freshwater environment. Most are from species living euplanktonically, but also several benthic species or epiphytic species exist.

Because of the sparse taxonomic criteria offered by the types of chrysophyte resting spores encountered in WW201216 and WW201217, the scarceness of such cysts in these sediments, and the fact that the cyst shape is not clearly species specific, a

taxonomic determination was not attempted. But their presence of course is an indication that the sediment was deposited in an aquatic environment.

In addition the fact is of importance that resting spores of chrysophyte algae are also relatively dissolution resistant biogenic siliceous components.

4.2.10 Silica diagenesis

While all these biosiliceous components are relatively rare, the silt fraction often has besides detrital minerals a third component group: zeolites (Figure 14, Figure 15, Appendix 11.4), and this component can be dominant in the silt fraction. Most frequent among the zeolites are clinoptilolite/ heulandite and analcime. Both show clear crystal shape, thus are authigenically formed.

In the more sandy samples on top of the clay-rich core interval as well as in the uppermost part of the clay-rich core interval these authigenic zeolites are especially prominent and large. In the lower part of the clay-rich core interval analcime is less abundant but clinoptilolite still is abundant in the silt fraction, though often with smaller crystals. The clinoptilolites are often heavily etched indicating ongoing dehydration and transformation into other authigenic minerals.

The precipitation of these zeolites is known from lakes in closed basins which during arid periods become alkaline and develop a high pH. This suggests also for the lake into which the Cubango Megafan was shed that it was a closed lake basin, its waters at times becoming increasingly alkaline and higher in pH. This is supported by the findings of the diatom species *Cyclotella meneghiniana* in the uppermost part of the clay-rich core interval, a species which is indicative of weakly alkaline waters. The occurrence of these two indicators next to each other implies short-term, possibly cyclic changes in lake volume and alkalinity and pH, be it annual cycles or cycles of longer duration.

For the samples within the clay-rich core interval the results of Kaufhold & Dohrmann (2009a; 2010) show that the clay minerals are nearly exclusively smectite. The pureness of this clay mineral, the association with the authigenic zeolites, and the inverse correlation of clay-sized material and siliceous microfossils indicates that also the smectite is a diagenetic product and formed in situ in the lake or marginally, not far away, being transported into the lake possibly by floods.

There is a difference in the authigenically formed minerals between the lower and the upper part of the clay-rich interval. In the lower part the abundance of the clay minerals is prominent and repeatedly reaches very high values, authigenically formed zeolites are characteristic of the silt fraction. In the upper part of the clay-rich interval authigenically

formed zeolites are dominant in the silt fraction, the clay fraction decreases, but smectite is still the dominant clay mineral here Kaufhold & Dohrmann (2009a; 2010).

4.3 Summary

The few test samples analyzed in this report can only provide general results. In addition these test samples have been used to test which methods are most suitable to obtain detailed and quantitative results on a set of more closely spaced samples. The general results obtained so far are:

4.3.1 Depositional environment of the sediments

- At least for large parts of the sediment sequence sedimentation occurred under aquatic conditions as documented by the presence of diatom valves and frustules, sponge spicules, and resting spores of chrysophycean algae.
- The aquatic environment was a large freshwater lake as documented by the diatom species and genera encountered as well as by the occurrence of remains of freshwater sponges. From biosiliceous remains no indications of a marine ingression could be detected.
- At least for the times when the earliest and especially when the latest sediments of the clay-rich core interval were deposited grass phytoliths are abundant and reflect extensive grass land in the surrounding of the lake. Also the presence of palms and other trees and shrubs is documented by phytoliths.
- The scarcity and the restricted occurrence of a fully planktonically living diatom species to site WW201216 suggests that WW201216 was located further towards the centre of the lake than WW201217.
- The presence of the remains of different species of the epiphytically living diatom genus *Epithemia* in sediments above and below the aquitard interval in borehole WW201217 prove, a) the presence of large water plants at the fringes of the lake at these times of sedimentation, b) the location of site WW201217 relatively close to the lake shore at these times, c) that the present difference of 21 m in elevation of the two site locations represents the former difference in depth in lake Etosha.
- For the uppermost part of the clay-rich interval alternations of weakly and strongly alkaline conditions are documented by a) the presence of the diatom species *Cyclotella meneghiniana* indicating weakly alkaline lake water at some times, b) the dominance of the authigenically formed zeolites, clinoptilolite/heulandite and

analcime in the silt fraction indicates alkaline conditions and a high pH followed by phases of intense freshwater inflow.

- The probable correlation between the natural gamma values and the abundance of the clay-fraction indicates that to a large part the natural gamma curve reflects the abundance of clay minerals in the sediment.
- The cyclic changes in natural gamma values within the aquitard interval of the cores reflect climatically controlled changes in diagenesis.
- How far the absence of diatoms in the central part of the aquitard interval of the two boreholes is due to silica dissolution or how far it documents a phase when the shrinking lake caused inhibiting conditions for diatoms or even its marginal parts fell dry, cannot be answered with the few samples checked at present.

4.3.2 Age of the deposits

The presence of the centric diatom genus *Cyclotella* as well as the dominance of opal phytoliths of C4-grasses means that sedimentation of this deltaic sequence occurred somewhere within the time interval from Middle Miocene to sub-recent.

4.3.3 Genesis of the aquitard:

Grain size analysis demonstrated that the raised natural gamma values in the aquitard interval are correlated to increased abundance of clay-sized sediment. The high abundance of authigenically formed zeolites (clinoptilolite and analcime dominant) in the silt fraction prove increased silica diagenesis under alkaline conditions and high pH for the clay-rich interval and surrounding. This together with the inverse correlation of clay-sized particles and siliceous microfossils suggests that also the clay-sized material in this core interval, which according to Kaufhold & Dohrmann (2009, 2010) is nearly exclusively smectite, is a result of this intense silica diagenesis.

Analysis of closer spaced samples is necessary to be able

- to evaluate the dissolution of the biosiliceous components and their contribution to the obvious silica diagenesis that created the aquitard, and
- to trace in detail the climatic fluctuations, which led to the fluctuating lake level and fluctuating alkalinity and pH.

Acknowledgements:

B. Piesker is thanked for the quantitative preparation of the samples for diatom analysis.
D. Klosa and S. Stäger are thanked for help with the SEM-work.
S. Kaufhold and K.P. Burgath are thanked for discussions concerning zeolite identification
D. Weck is thanked for XRD-analysis of the ungrinded grain size fraction 20-32 µm.

5 Discussion and Conclusion

The investigation of the sedimentary history of the Cubango Megafan is still an ongoing process within this project. An important step towards the understanding has been contributed by (Fenner, 2010) and Dill et al. (2012, see Appendix 1.6). Therefore, results and the conclusion of this report are still preliminary and hence rather meant to give a short overview and summary of findings from the different sample investigations, especially the ones which were not documented in an additional short report.

Van Wyk (2009a, Appendix 1) defined zones of aquifers and aquitards according to his lithologs and the geophysical logs (see also Figure 13 of Report Part A). This system of three aquifers is based on general knowledge of the aquifer system of the Cubango Megafan (Bittner and Kleczar, 2006). These are namely from top to bottom, the Discontinuous Perched Aquifer (KDP or KOH-0), the Upper Ohangwena Aquifer (KOH-1) and Lower Ohangwena Aquifer (KOH-2); K stands for aquifers in the Kalaharie Group. The KDP is an expression for perched aquifers in the CEB in general, for detailing specific characteristics; it will be called KOH-0 on the Cubango Megafan. Walzer (2010) additionally divides the aquitard between KOH-1 and KOH-2 in three sub-sections at WW201045. The middle section contains a higher clay content than the encompassing sections and has a lower hydraulic conductivity. This division (Table 7) is based on the visual interpretation of lithologs and geophysical logs as well as measured hydraulic conductivities. It is also reflected in mineralogical characteristics, but Dill et al. (2012) show that lithofacies types tell a broader story of the distribution of aquifer and aquitards. The difficulty of interpretation of results and zonation of stratigraphic and hydrostratigraphic units lies within the lack of sharp borders within the sediment columns, as well as in the low density of information in its spatial distribution. It has to be taken into account that the Cubango Megafan covers an area of about 55.000 km^2 with 35.000 km^2 in Namibia alone and that two well investigated borehole location exist so far. Within the realm of the megafan, the spatial heterogeneity of sediments is enormous and it is not yet possible to determine local distribution of specific layers. However, two general trends are observable:

1. A rough zonation into three aquifers and three aquitards is possible in the western part of the Cubango Megafan.
2. Lithofacies types as described in Dill et al. (2012) show an influence from the depocenter in the CEB (the border of the megafan) towards the proximal part of the Cubango Megafan.

Hence a certain spatial distribution can be concluded by sedimentological symmetries but caution needs to be applied.

The mineralogical content of the samples from borehole WW201216 which are from a depth between 127 to 266 meters is mainly quartz and feldspar, also zeolites and carbonates could be identified. All samples contain clay minerals. However, samples below a depth of 230 m have significant lower signals for illite and smectite, which is correspondent to aquifer unit KOH-2. Traces of pyrite are noteworthy in a depth of 248.5 m. According to the cation exchange capacity (CEC), the smectite content is about 20 % in the clay rich layer from a depth of 200-230 m. The smectites do not have an unusual composition like the ones in the drill bit sample (see Chapter 3.4.2). Porosity of smectite rich samples is similar to porosity of other samples. However, this is due to the determination method which is conducted in a state where smectite minerals are dry. The smectites are dominantly found in the pores of the sand grains as REM pictures show. A dominance of Na over Ca and Mg smectites explains the building of low density (soft) gels of smectites with water.

Table 7: Naming and interpretation of hydrostratigraphic units of the Cubango Megafan after (Bittner and Kleczar, 2006; Miller, 2008b; Miller et al., 2010; Walzer, 2010).

Hydrostratigraphic Unit (Bittner and Kleczar, 2006; Walzer, 2010)	Description	Lithofacies Unit (Dill et al., 2012)
KDP/ KOH-0	Possibly discontinuous perched Aquifer in aeolian sediments of the Cubango Megafan	**Suggested: VIII**
KOH-S1	Aquitard between KOH-O and KOH-1	**VI – VII?***
KOH-1	Upper Aquifer system of the Cubango Megafan, this aquifer has increasing salinity towards the depocenter of the CEB and is not a single unit with high yield but a quite heterogeneous system of small scale aquifers and aquitards. According to (Bittner and Kleczar, 2006) this aquifer belongs to the Andoni Formation.	**V – VII?***
KOH-S2	An approximate 100 m thick layer of low hydraulic conductivity with some sub-units as defined by Walzer (2010). Salinity is elevated in relation to KOH-1 in the east of the Cubango Megafan. In WW201045 three sub-units are identified, the middle unit has clearly elevated clay contents and shows stronger signals of magnetic susceptibility. This unit is possibly found in other wells but not in WW201047.	**III – IV, V?***
KOH-2	Distinct freshwater aquifer whose salinity increases according to KOH-1 but the freshwater reaches laterally further towards the depocenter. The aquifer reaches approximately from 200-300 meters and was found in WW201045-WW201047 and with elevated salinities also in WW201345. According to (Bittner and Kleczar, 2006) this aquifer belongs to the Olukonda Formation.	**Ib – II**
KOH-S3	Aquitard with increased clay content, found in WW201045 and WW201047.	**Ia**

* aquifers and aquitards might occur in units with question marks, according to the spatial distribution.

The mineralogical content of the 11 samples from borehole WW201217 which lie within a depth of 90 to 240 meters, span a wider variety of sedimentological units than the samples in borehole WW201216. Three general systems can be recognized that coincide with the upper aquifer KOH-1, the aquitard and the lower aquifer KOH-2: In the zone of elevated gamma counts between 105 and 200 meters, additional minerals are found, e.g. smectites. They show different morphologies that indicate different origin of parent materials. In the top to a depth of 105 m, feldspar is missing but Clinoptilolite is found. Clinoptilolite is a diagenetic product often but not always from alteration of volcanic rocks or fragmental debris (International Zeolite Association, 2012). Authigenic Clinoptilolite can develop in saline to alkaline lakes in arid environments. Below a depth of 200 m, feldspar is found but carbonates and clay minerals were not detected. The three different sections resemble the breakthrough of the Kunene Megafan as described by Dill et al. (2012).

In comparison to WW201216, borehole WW201217 shows more distinct boundaries between an upper, middle and lower section that is most pronounced in the gamma ray log of WW201217. The upper section comprises the aquifers and aquitards KOH-0 to KOH-1 (Table 7). The middle section is equivalent to the aquitard above KOH-2. It is evident that the clay rich sections found in WW201216 does not exist in WW201217. It is either not deposited or has been eroded and is missing in the logs at the hiatus which pronounces the changes of the gamma ray log. In both sample sets, the Cation Exchange Capacity corresponds with the porosity of each sample. In addition to this, the significant border from aquitard to aquifer KOH-2 is in WW201217 about 40 m higher than in WW201216 which is located more distal on the megafan.

The major and minor element content analysis in cutting samples of WW201045 shows several sequences and general trends within the sedimentation history (Dill et al., 2012). The grain size distribution has a bimodal character. The fine grain sizes are dominant due to the re-mineralization of smectites (Figure 8). Other than that, fine to medium sand is dominant. The log of main and trace elements shows a series of periods that are interrupted by hiatuses (Dill et al., 2012)Figure 17). A general trend of increasing silica content towards the top is observable as well as elevated clay content in the aquitard.

The seven stratigraphic units or lithofacies types respectively and some sub-units that have been identified according to Dill et al. (Dill et al., 2012) give an idea about the spatio-temporal evolution of the sediments (Figure 17) and the prevailing lithofacies from bottom to top.

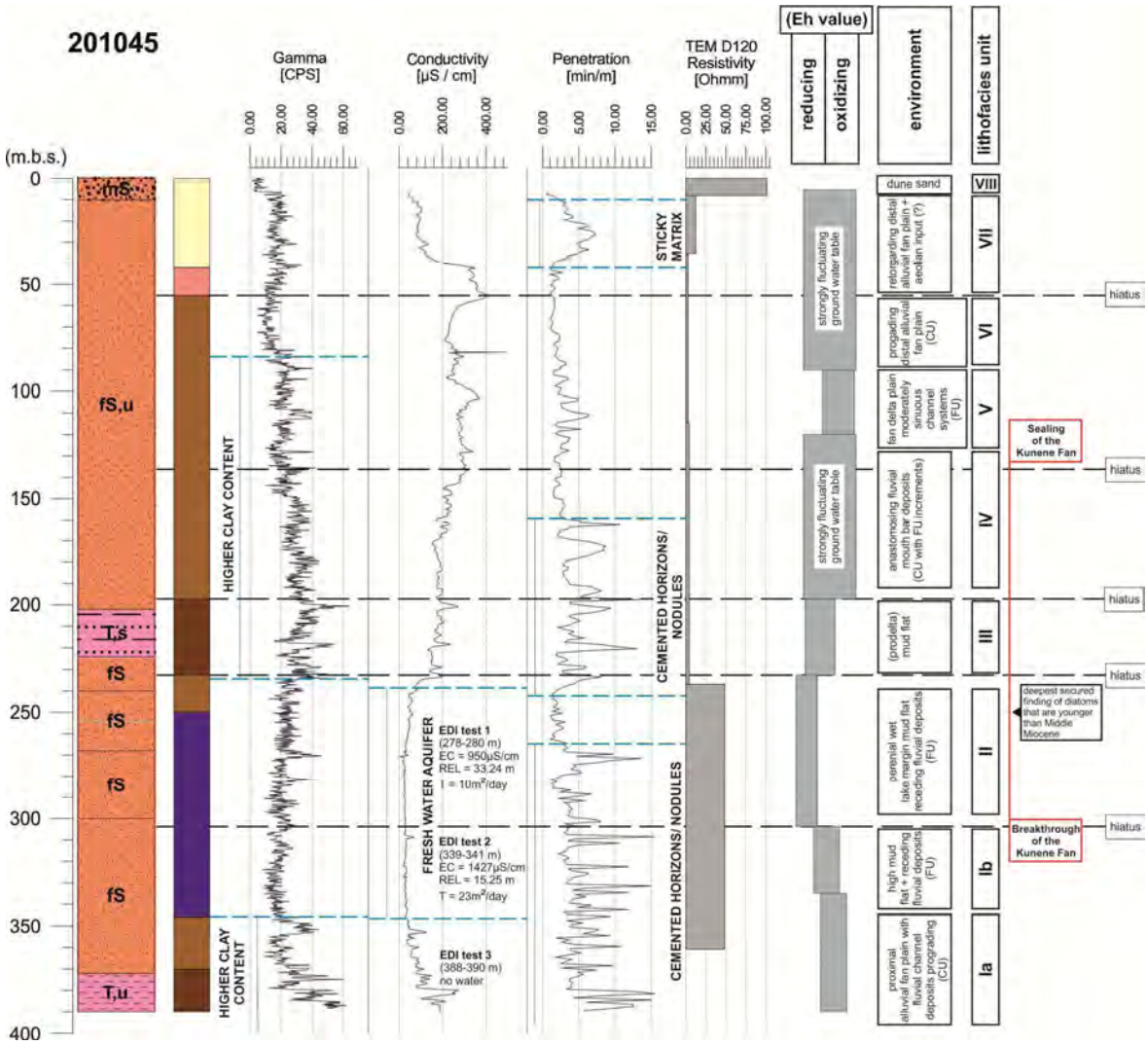

Figure 17: Lithofacies units according to Dill et al. (Dill et al., 2012). Litholog: (Miller, 2010); hydrogeological units: (Walzer, 2010); gamma and conductivity logs of geophysical logging campaign I, see volume Ib: (Lindenmaier et al., 2012); penetration was recorded in min/m by hand logging; TEM profile from Schildknecht (2012); Eh-value, environment and lithofacies unit from Dill et al. (2012), Eh-value represents potential conditions during sedimentation.

Lithofacies I: Lithofacies Ia describes a proximal alluvial fan plain with prograding fluvial channel deposits. The gamma and conductivity logs show elevated clay mineral contents and a possibly elevated pore fluid content. The alluvial fan deposits then change towards high mud flat and receding fluvial deposits on top in Lithofacies Ib. Gamma and conductivity logs show decreased clay contents and fluid ionization. The change of the lithofacies in-between Ia and Ib is the lower border towards the aquifer KOH-2.

Lithofacies II is characterized by sediments of a perennial wet lake margin, mud flats and receding fluvial deposits. The penetration log shows a raised amount of cemented horizons. It represents the upper part of the freshwater zone with low gamma and

conductivity signals. The term “mud flat” of lithofacies Ib and II should not be taken too literally, the recent Okavango delta shows that the accumulation of clay or organic material is not a must for these kind of environments (Stanistreet and McCarthy, 1992), it is rather a description of the kinetic characteristics and could be compared as a “sand flat”.

Lithofacies III presents the progradation of megafan series with characteristics of a losimean fan as defined by (Stanistreet and McCarthy, 1992). Massive fine grained sands with elevated clay contents are found. Drill sites 201047 and 201046 attest to an interfingering of mud flats and lacustrine deposits while drill site WW201346 represents the opposite end by a saline lake facies. Gamma and conductivity values are elevated.

Lithofacies IV and V represent sediments of a low-gradient fan and changes in between anastomosing and meandering fluvial deposits. Both facies are characterized by elevated gamma signals but V shows slightly elevated conductivity values. Heavy minerals suspect an influence of the Cunene within lithofacies II through IV.

Lithofacies VI and VII may be interpreted as a retrograde distal alluvial fan plain with some aeolian reworking, associated by the formation of pediments and glacis near the hinterland.

An additional, uppermost facies (Lithofacies VIII) is of aeolian origin and but was not recorded in samples at borehole site WW201045. According to (Miller et al., 2010) these white sands are reworked Kalahari sediments and are overlain by thin longitudinal reddish dune sands. It is assumed that these dunes accumulated in the period when the Etosha Pan was excavated (Buch, 1997; Buch and Trippner, 1997).

Preservation of microfossils is low in sand rich samples, some higher fossil content can be expected in samples with a higher content of silt and clay sized grains. Besides skeletal remnants of plants (phytoliths), siliceous remains of aquatic living organisms were found: algae and spicules of sponges. The siliceous remnants of the algae are valves of benthic, planktonic and tychoplanktonic diatoms and resting spores of *Chrysophyceae*. Phytoliths were found in all samples and are the most abundant species. An investigation of recent grass ecosystems would help to find paleo-environmental indicators in the samples. Most abundant are phytoliths of grasses that exist in tropical and subtropical regions with low to moderate soil moisture. The dominance of remains of C4-grasses suggests that the age of the deposits lies somewhere in the time interval from middle Miocene to Recent.

Taxonomic determination clearly showed that all tested samples contain freshwater diatoms. One single find indicates a deeper lake environment. One other finding is

reported to be characteristic for weakly alkaline saline lakes. At a certain time a shallow lake environment must have persisted which gave a habitat for such water plants. Principally, samples of WW201216 have characteristics of a slightly wetter environment than samples of WW201217 which is also more proximal on the Cubango Megafan. Normally, clay rich layers have a higher fossil content than sandy layers. Here, it is vice versa which can be explained by stronger silica diagenesis in the clay layers.

The results of detailed borehole investigation show that combined sedimentological, paleontological and hydrogeological (including geophysics) investigation greatly helps to delineate the aquifer system of the Cubango Megafan. Although not finalizing this effort, the current results support general knowledge of the aquifer system and reveal a complicated interaction of paleo-environments (including paleo-climate) and nowadays groundwater distribution. Further synthesis of results is ongoing. In addition, the first core sampling revealed that additional material should be investigated, so that currently more than 70 samples are investigated within the Kalahari research project of BGR.

6 References

Baker, G., 1959. Opal phytoliths in some Victorian soils and “red rain” residues. Australian Journal of Botany, 7: 64-87.

Baker, G., 1960. Fossil opal-phytoliths. Micropaleontology, 6(1): 79-85.

Battarbee, J.R., 1973. A new method for the estimation of absolute microfossil numbers, with reference especially to diatoms. Limnol. Ocean, 18: 647-652.

Bittner, A.F.W., Kleczar, M.L., 2006. Desk Study Report: Cuvelai-Etosha Groundwater Investigation, Bittner Water Consult, Windhoek, Namibia.

Buch, M.W., 1997. Etosha pan - the third largest lake in the world? Madoqua, 20: 49-64.

Buch, M.W., Trippner, C., 1997. Overview of the geological and geomorphological evolution of the Etosha region, northern Namibia. Madoqua, 20: 65-74.

de Araújo, A.G., Perevalov, O.V., Jukov, R.A., 1988. Carta geológica de Angola. Instituto Nacional de Geologia de Angola, pp. Scale: 1:1.000.000, Coordinates S180000 S070000 E0240000 E0120000.

Dill, H. et al., 2012. Joint clay-heavy-light mineral analysis: a tool to investigate the hydrographic-hydraulic regime of Late Cenozoic deltaic inland fans under changing climatic concitions (Cuvelai-Etosha Basin, Namibia). International Journal of Earth Science.

DIN EN 12457-4, 2003. Characterization of waste - Leaching; Compliance test for leaching of granular waste materials and sludges - Part 4: One stage batch test at a liquid to solid ratio of 10 l/kg for materials with particle size below 10 mm (without or with limited size reduction). German Industry Norm.

Fehr, A., 2007. NMR und SIP Messungen an Gesteinsproben, RWTH Aachen, Aachen, 114 pp.

Fenner, J., 2010. Silt fraction analysis of the boreholes NAM 201216 and 201217, Namibia and its indications for palaeoenvrionment and sediment age, Bundesanstalt für Geowissenschaften und Rohstoffe, Germany.

Geological Survey of Namibia, Simplified geological map of Namibia <1:2000000>. In: Namibia, G.S.o. (Ed.), Windhoek, pp. Scale: 1:2000000, Coordinates: S290000 S165000 E0251000 E0114500.

Haddon, I.G., 2005. The Sub-Kalahari Geology and Tectonic Evolution of the Kalahari Basin, Southern Afrika, University of Witwatersrand, Johannesburg, 360 pp.

Hecky, R.E., Kilham, P., 1973. Diatoms in alkaline, saline lakes: ecology and geochemical implications. Limnology and Oceanography, 18(1): 53-71.

Hipondoka, 2005. The Development and Evolution of Etosha Pan, Namibia

International Zeolite Association, 2012. Characteristics of Clinoptilolite, http://www.iza-online.org/natural/Datasheets/Clinoptilolite/Clinoptilolite.html.

Kaufhold, S., Dohrmann, R., 2009a. Clay mineralogical characterisation of a clay sample from Namibia.

Kaufhold, S., Dohrmann, R., 2009b. Mineralogical characterisation of samples from drill hole 201216, Namibia.

Kaufhold, S., Dohrmann, R., 2010. Mineralogical characterisation of samples from drill hole 201217, Namibia.

Krebs, W., Bradbury, J., 1995. Actinocyclus (Bacillariophyta) species from lacustrine Miocene deposits of the western United Staates. U.S. Geol. Surv. Prof. Paper, 1543 A-B: 1-15.

Kringel, R., Hoffmann, S., 2008. Datenmanagement und dreidimensionales, hydrogeologisches und hydrogeochemisches Untergrundmodell (Abschlussbericht Teilprojekt 2) im KORA Themenverbund 3 : raumdifferenziertes innovatives Monitoring von LCKW - Grundwasserkontaminationen am Beispiel von Hannover-Südstadt Hannover.

Meier, L.P., Kahr, G., 1999. Determination of the cation exchange capacity (CEC) of clay minerals using the complexes of Copper (II) ion with Triethylenetetramine and Tretraethylenepentamine. Clays and Clay Minerals, 47: 386 - 388.

Mendelsohn, J., El Obeid, S., Roberts, G., 2000. A profile of north-central Namibia. Environmental profiles project. Gamsberg Macmillan Publishers, Windhoek, 80 pp.

Miller, R., 2008a. The Geology of Namibia - Volume 1 - Archaen to Mesoproterozoic, 1. Ministry of Mines and Energy, Geological Survey, Windhoek.

Miller, R., 2008b. The Geology of Namibia - Volume 3 - Palaezoic to Cenozoic, 3. Ministry of Mines and Energy, Geological Survey, Windhoek.

Miller, R.M., 1997. The Owambo Basin of Northern Namibia. In: Selly, R.C. (Ed.), African Basins, Sedimentary Basins of the World. Elsevier Science B.V., Amsterdam, pp. 237-268.

Miller, R.M., 2010. Lithology of boreholes WW 201216 and WW 201217, Ohangwena region, Namibia.

Miller, R.M., Pickford, M., Senut, B., 2010. The Geology, Palaeontology and Evolution of the Etosha Pan, Namibia: Implications for Terminal Kalahari Deposition. South African Journal of Geology, 113(3): 307-334.

Miller, R.M., Schalk, K.E.L., 1980. Namibia : geological map <1:1000000>. In: Namibia, G.S.o. (Ed.), pp. Scale: 1:1000000, Coordinates: S290000 S165500 E0213600 E0111320.

Mulder, C., Ellis, R.P., 2000. Ecological significance of South-West African grass-leaf phytoliths: a climatic response of vegetation biomes to modern aridification trends. Grasses: systematics and evolution, 1998. CSIRO Melbourne, 248-258 pp.

Ognjanova-Rumenova, N.G., 2000. Lacustrine diatom flora from Neogene basins on the Balkan Peninsula: preliminary biostratigraphical data. The origin and early evolution of the diatoms: fossil, molecular and biogeographical approaches. W. Szafer Institute of Botany, Polish Academy of Sciences, Cracow, 137-143 pp.

Runge, F., 1999. The opal phytolith inventory of soils in central Africa – quantities, shapes, classification, and spectra. Review of Palaeobotany and Palynology, 107: 23-53.

Sandgren, C.D., 1983. Morphological variability in populations of chrysophycean resting cysts. I. Genetic (interclonal) and encystment temperature effects on morphology. . J. Phycol., 19: 64-70.

Schildknecht, F., 2012. Groundwater for the North of Namibia - Groundwater exploration with TEM soundings in the Cuvelai-Etosha-Basin - Report Part C, in preparation.

Stanistreet, I.G., McCarthy, T.S., 1992. The Okavango Fan and the classification of subaerial fan systems Sedimentary Geology, 85: 115-133.

Twiss, P.C., Suess, E., Smith, R.M., 1969. Morphological classification of grass phytoliths. Soil Science of America, Proceedings 33: 109-115.

Vanhala, H., Soininen, H., 1995. Laboratory technique for measurement of spectral induced polarization response of soil samples Geophysical prospecting, 43(5): 655-676.

Walzer, A., 2010. Multilayered Aquifers in the Central-North of Namibia and their Potential Use for Water Supply, Technische Universität Dresden, Bundesanstalt für Geowissenschaften und Rohstoffe.

Webb, P.A., Orr, C., 1997. Analytical methods in fine particle technology. . Micromeritics Instrument Corp, , Norcross GA, USA, 301 pp.

Wyk, B., 2009a. Drilling report for three deep boreholes in the Cuvelei-Etosha Basin.

Wyk, B., 2009b. Rural Water Supply Drilling Program 2009 - Ohangwena Region, Bittner Water Consult CC.

Zauter, H., personal communication. Project Leader BGR 2007-2010.